Phylogenomics of 8,839 *Clostridioides difficile* genomes reveals recombination-driven evolution and diversification of toxin A and B

Michael J. Mansfield[1*], Benjamin J-M Tremblay[1*], Ji Zeng[2,3], Xin Wei[1], Harold Hodgins[1], Jay Worley[4,5], Lynn Bry[4,6], Min Dong[2,3,#], Andrew C. Doxey[1,#]

[1]Department of Biology, David R. Cheriton School of Computer Science, and Waterloo Centre for Microbial Research, University of Waterloo, 200 University Ave. West, Waterloo, Ontario, N2L 3G1, Canada.

[2] Department of Urology, Boston Children's Hospital, Boston, Massachusetts, USA

[3] Department of Microbiology, Harvard Medical School, Boston, Massachusetts, USA

[4] Massachusetts Host-Microbiome Center, Department of Pathology, Brigham and Women's Hospital, Harvard Medical School, Boston, MA, USA

[5] National Center for Biotechnology Information, National Library of Medicine, National Institutes of Health, Bethesda, MD, USA

[6] Division of Infectious Diseases, Department of Medicine, Brigham and Women's Hospital, Harvard Medical School, Boston, Massachusetts, USA

[*]Co-first authors

[#]Correspondence should be addressed to A.C.D. (acdoxey@uwaterloo.ca) and M.D. (min.dong@childrens.harvard.edu)

Abstract

Clostridioides difficile is the major worldwide cause of antibiotic-associated gastrointestinal infection. A pathogenicity locus (PaLoc) encoding one or two homologous toxins, toxin A (TcdA) and toxin B (TcdB) is essential for *C. difficile* pathogenicity. However, toxin sequence variation poses major challenges for the development of diagnostic assays, therapeutics, and vaccines. Here, we present a comprehensive phylogenomic analysis 8,839 *C. difficile* strains and their toxins including 6,492 genomes that we assembled from the NCBI short read archive. A total of 5,175 *tcdA* and 8,022 *tcdB* genes clustered into 7 (A1-A7) and 12 (B1-B12) distinct subtypes, which form the basis of a new method for toxin-based subtyping of *C. difficile*. We developed a haplotype coloring algorithm to visualize amino acid variation across all toxin sequences, which revealed that TcdB has diversified through extensive homologous recombination throughout its entire sequence, and formed new subtypes through distinct recombination events. In contrast, TcdA varies mainly in the number of repeats in its C-terminal repetitive region, suggesting that recombination-mediated diversification of TcdB provides a selective advantage in *C. difficile* evolution. The application of toxin subtyping is then validated by classifying 351 *C. difficile* clinical isolates from Brigham and Women's Hospital in Boston, demonstrating its clinical utility. Subtyping partitions TcdB into binary functional and antigenic groups generated by intragenic recombinations, including two distinct cell-rounding phenotypes, whether recognizing frizzled proteins as receptors, and whether can be efficiently neutralized by monoclonal antibody bezlotoxumab, the only FDA-approved therapeutic antibody. Our analysis also identifies eight universally conserved surface patches across the TcdB structure, representing ideal targets for developing broad-spectrum therapeutics. Finally, we established an open online database (DiffBase) as a central hub for collection and classification of *C. difficile* toxins, which will help clinicians decide on therapeutic strategies targeting specific toxin variants, and allow researchers to monitor the ongoing evolution and diversification of *C. difficile*.

Key words: C. difficile, toxin, TcdA, TcdB, toxin A, toxin B, recombination, subtype, bezlotoxumab, frizzled

55 **Introduction**

56

57 *Clostridioides difficile* (formerly *Clostridium difficile*) is a diverse group of Gram-positive spore-
58 forming anaerobic bacteria[1]. Toxigenic strains have become important opportunistic pathogens to
59 humans. Their spores are widespread and can colonize human and animal colons after disruption
60 of the gut microflora, most notably due to antibiotic treatment. *C. difficile* infection (CDI) results
61 in a range of symptoms from self-limiting diarrhea to severe pseudomembranous enterocolitis and
62 death[2–7]. It is the most frequent cause of healthcare-associated gastrointestinal infections across
63 developed countries worldwide[2–5,8].

64

65 Ribotyping (RT), which compares intergenic spacers between ribosomal RNA genes, is widely
66 utilized to categorize *C. difficile* linages[5,9]. Various other methods including multilocus sequence
67 typing based on allelic variation of housekeeping genes and whole genome sequencing analysis
68 have also been adopted to further discriminate strains[5,9–13]. Phylogenetic analyses revealed a
69 growing diverse population[1,14–16]. In recently years, there is an emergence and spreading of various
70 epidemic hypervirulent strains such as the RT027 clonal linage, which first caused outbreaks in
71 2000-2003 in North America and is associated with increased disease severity and mortality[17–20].
72 RT078 is an emerging hypervirulent linage which is also the dominant type found in domesticated
73 animals[21,22]. There are also geographic differences, for instance, RT017 has become a dominant
74 lineage in Japan and Korea[23].

75

76 The major virulence factors in toxigenic *C. difficile* strains are two homologous large protein
77 toxins, TcdA (~300 kDa) and TcdB (~270 kDa)[24–27]. Nontoxigenic *C. difficile* strains without these
78 toxins exist and can colonize humans and animals, but do not cause diseases[28]. TcdA and TcdB
79 share overall ~66% sequence similarity and belong to the large clostridial toxin (LCT) family,
80 which include TcsH and TcsL in *Paeniclostridium sordellii*, Tcnα in *Clostridium novyi*, and TpeL
81 in *Clostridium perfringens*[5,6,8,9,24,25,29–31]. TcsH and TcsL can be considered orthologs of TcdA and
82 TcdB, respectively, with TcsH sharing ~77% sequence identity with TcdA and TcsL sharing ~76%
83 identity with TcdB[32] (Fig. S1). TcdA and TcdB share a protein domain architecture consisting of
84 an N-terminal glucosyltransferase domain (GTD), followed by a cysteine protease domain (CPD),
85 an intermingled membrane translocation delivery domain and receptor-binding domain (DRBD),

86 and a large C-terminal combined repetitive oligopeptides domain (CROPs) (Fig. S1). After
87 binding, endocytosis, and translocation across endosomal membranes into the cytosol of host cells,
88 these toxins glucosylate and inactivate host Ras/Rho family of small GTPases, leading to
89 disruption of the actin cytoskeleton, cell rounding, and ultimately cell death[33].
90
91 TcdA and TcdB were first identified in the 1990s, and the toxin sequences from a reference strain
92 (VPI10463) have been widely used as the standard in diagnostic and therapeutic development.
93 However, sequence variations in the toxin genes exist across *C. difficile* strains and could affect
94 receptor-binding specificity, preferences toward distinct small GTPases, overall toxicity, and
95 antigenicity. For instance, strains such as R20291 (belonging to RT027) produces a TcdB variant
96 with ~8% of residue differences from the reference TcdB, which exhibited a significant impact on
97 its immunogenicity: mice immunized with the reference TcdB developed resistance to the same
98 TcdB, but all died when challenged with this variant TcdB[34], and several antibodies raised against
99 the reference TcdB, including the FDA approved therapeutic antibody bezlotoxumab, either do
100 not recognize or have lower efficacy against this TcdB variant[34–36]. Furthermore, this TcdB variant
101 also loses the ability to recognize frizzled (FZD) proteins, which are one of the major receptors for
102 the reference TcdB, due to residue changes at the FZD-binding interface[35,37–40].
103
104 These toxin variations pose a significant challenge for developing effective broad-spectrum
105 diagnostic assays, therapeutic antibodies, and vaccines. Understanding variations in toxins is a key
106 step to address this challenge and may also reveal their potential evolutionary paths and functional
107 differences. A toxinotyping method has been previously developed utilizing PCR-based
108 amplification of toxin gene fragments and analyzing polymorphism with restriction enzyme
109 digestions, which can distinguish over 34 toxinotypes[41,42]. Although toxinotyping highlights the
110 variation among toxin genes, it lacks the resolution to understand the molecular basis for
111 diversification of toxins and sequence-function relationships.
112
113 Rapid growth of genomic sequencing of *C. difficile* strains in recent years provides an opportunity
114 to analyze and categorize the diversification of TcdA and TcdB with single residue resolution.
115 Here we performed a comprehensive analysis of nearly all available *C. difficile* TcdA and TcdB
116 sequences, including assembly and analysis of 6,492 new genomes, with the goal to 1) build a

117 comprehensive central database of *C. difficile* toxin sequences; 2) better understand the
118 mechanisms underlying TcdA and TcdB diversification; and 3) develop a system to classify TcdA
119 and TcdB into subtypes that allow clinicians and researchers to categorize and predict functional-
120 immunological variations of any future sequenced *C. difficile* isolates.
121

Results

Collection of TcdA and TcdB sequences across 8,839 C. difficile genomes

To build a comprehensive database of TcdA and TcdB sequences, we combined data from NCBI GenBank and the NCBI short-read archive (SRA). From 2,347 *C. difficile* genomes in GenBank, we identified an initial set of 1,633 *tcdA* and 2,028 *tcdB* genes. We then developed a computational pipeline for automated retrieval of *C. difficile* genomes from the SRA, *de novo* genome assembly, genome annotation, and extraction of *tcdA* and *tcdB* genes (see Methods). Using this pipeline, we assembled the genomes of 6,492 *C. difficile* isolates and identified an additional 3,542 *tcdA* and 5,994 *tcdB* genes (Table 1). Combining both sources, we identified 5,175 TcdA and 8,022 TcdB encoding sequences.

We then carried out alignments of all toxin protein sequences. The TcdB alignment covered the entire sequence (1-2366), with 712 (30%) of the positions showing variations across all domains. The TcdA alignment possessed much lower variation than TcdB within the 1-1874 region as it had only 168 (9%) variable sites, but its CROPs domain (1831-2710) contained an extremely high degree of variation in the number length of repeats: from 3 repeats in the shortest variant to 45 in the longest variant, and 32 in the reference TcdA variant from VPI 10463 (Fig. S2). This is likely generated by homologous recombination due to the repetitive nature of this region. The CROPs domain is composed of long repeats (LRs) of ~30 residues and short repeats (SRs) of ~19-24 residues[27]. The CROPs domain in TcdA is not only repetitive at a protein sequence level, but also showed a high degree of repetitiveness at a DNA level, whereas the repetitiveness of the CROPs domain in TcdB is largely limited to the protein level[43,44], which may account for frequent recombination in TcdA-CROPs but not in TcdB-CROPs.

Classifying TcdA and TcdB into subtypes

In total, there were 116 unique TcdA protein sequences and 212 unique TcdB protein sequences. We then clustered these sequences into distinct subfamilies ("subtypes") using average linkage hierarchical clustering (see Methods). Analysis of TcdB is based on full-length sequences, but

153 TcdA is limited to the 1-1874 region to avoid the highly variable CROPs domain. In addition, we
154 also included TcsH and TcsL sequences in our analysis. Clustering produced 7 distinct TcdA
155 subtypes which we labeled A1-A7, and 12 distinct TcdB subtypes which we labeled B1-B12, with
156 the subtype number ranked based on their total frequency of occurrence in GenBank and NCBI-
157 SRA (Fig. 1). Each unique sequence was then further numbered following a period within its
158 subtype (e.g. B1.1, 1.2, 1.3, etc.). Sequences within the same TcdA and TcdB subtype demonstrate
159 strong pairwise similarities, and weak similarities between subtypes (Fig. 1a, 1d). Quantitative
160 analysis revealed that thresholds of 99.4% (TcdA) and 97% (TcdB) can be used to effectively
161 assign toxin sequences to these subtypes (Fig. S3). We then selected one representative sequence
162 for each subtype and carried out phylogenic analysis and pairwise comparison. TcdA subtypes A1
163 to A6 possess higher similarities (>97.9%) and clustered together, with A7 forming a divergent
164 lineage (Fig. 1b, 1c). A7 is a unique sequence with only 85.3% to 85.6% identity to others (Fig.
165 1c). The entire TcdA family was further outgrouped by TcsH as expected (Fig. 1b). TcdB also
166 formed a monophyletic family that was outgrouped by TcsL and a second lineage of TcsL-related
167 proteins (Fig. 1e). TcdB subtypes can be subdivided into three groups, one including B6, B7, B4,
168 B8, a second including B9, B2, B10, B11, and a third including B12, B1, B5, and B3 (Fig. 1e).
169 The lowest identity among TcdB subtypes is 85.3% (between B7 and B12, Fig. 1f). A7, B10, B11,
170 and B12 represent rare divergent subtypes recently reported: A7 is in strain RA09-70, which does
171 not express TcdB[45]; B10, B11, and B12 were identified recently from strains CD10-165, CD160,
172 and 173070, respectively[45], and all three strains do not express TcdA.
173
174 By mining unassembled *C. difficile* genomes from the SRA, we were able to discover 125 TcdA
175 and TcdB protein sequences that were not represented in GenBank. Most novel toxin variants
176 clustered into subtypes A1 (N = 25), B1 (N = 52), and subtypes A2 (N = 10) and B2 (N = 12)
177 (Table S1). However, three highly divergent TcdA variants identified from SRA datasets formed
178 new subtypes not represented in GenBank. These include subtypes A4 from strain ECDC-088
179 (SRS1486236), A5 from strain ECDC-009 (SRS1486256), and A6 from strain L;13.7548369.T
180 (SRS1486661), all of which are clinical isolates. All three of these strains contained
181 truncated/partial TcdB variants which represent putative pseudogenes.
182

183 To link our subtyping with known clinical *C. difficile* strains, we manually curated subtype
184 assignments for a set of 63 *C. difficile* strains selected from the literature, which covers known
185 toxinotypes, and compared subtypes with toxinotypes, ribotypes, and whether the strain produces
186 the third toxin known as *C. difficile* transferase toxin (CDT) (Table S2). The majority express an
187 A1/B1 subtype combination and include reference strains 630 and VPI 10463 that express the
188 widely used standard TcdA and TcdB sequence (defined as A1.1 and B1.1, Table S2). The group
189 that expresses a combination of A2/B2 is the second largest and includes hypervirulent RT027
190 strains R12087 and R20291. The group expressing A3/B3 include strains (e.g. M120 and NAP07)
191 classified as RT078. Subtype B4 is mainly expressed in strains (e.g. 1470) belonging to RT017,
192 which lacks TcdA. Other pairings in the table include A2/B9, A3/B5, A2/B6, and A1/B4. The
193 table includes many strains that do not express functional TcdA, which can express B1, B2, B3,
194 B4, B6, B7, B8, B10, B11, or B12; one strain that only expresses TcdA but not TcdB (A7 in RA09-
195 70); four strains that only express CDT; and one strain (SLO037) that expresses none of the three
196 toxins. This table represents a small portion of *C. difficile* strains and a full list of a total 1640 *C.*
197 *difficile* strains from the NCBI database with their toxin subtypes noted is included as Table S3.
198
199 In general, phylogenetic subtyping of *C. difficile* toxins correlated well with previously identified
200 toxinotypes, but at greater resolution by analyzing TcdA and TcdB separately (Table S2, see
201 Discussion). There was less congruence with ribotypes, however, as different subtypes were found
202 in the same ribotype strains, and the same subtype was found in different ribotype strains.
203 Therefore, neither toxinotype nor ribotype were able to accurately categorize toxins based on
204 phylogenetic relationships (Table S2). Subtyping was capable of capturing the full phylogenetic
205 diversity of TcdA and TcdB available in previously known and new strains.
206
207
208 ***Distribution of toxin subtypes across the C. difficile phylogeny***
209
210 To evaluate the phylogenomic distribution of toxin subtypes across *C. difficile*, we constructed a
211 whole-genome based phylogeny of 1,934 complete *C. difficile* genomes based on 14,194 SNP
212 positions across 88 conserved marker genes (Fig. 2a, Table S3) (see Methods). The genome tree
213 is highly consistent with known phylogenetic relationships, as the previously identified clades 1-

214 5 are represented by distinct lineages[14] (Fig. 2a). Two of the three divergent environmental
215 lineages C-I and C-II are also present as divergent branches (Fig. 2a).
216
217 A total of 1,640 (84.8%) *C. difficile* strains were found to encode TcdA and/or TcdB, while the
218 remainder (294, 15.2%) lack toxin genes. The predicted toxin subtypes across the *C. difficile*
219 genome tree demonstrate strong clade associations, and therefore are highly congruent with strain
220 phylogenetic relationships. The congruency between subtype and phylogeny provides further
221 support for our toxin classification (Fig. 2a). For example, subtype A1/B1 which includes
222 reference strains 630 and VPI 10463 is most common among toxin-containing strains (979, 59.7%)
223 and associated with clade 1 (Fig. 2b). A2/B2 was second most common and associated with clade
224 2, A3/B5 with clade 3, -/B4 with clade 4, and A3/B3 with clade 5. Also prevalent were types -/B1,
225 A1/-, and A2/B6 (Fig. 2b). Deviations from the A1/B1 toxin type are often associated with the
226 emergence of numerous hypervirulent and epidemic outbreak strains such as A2/B2 (RT027),
227 A3/B3 (RT078), and -/B4 (RT017) (Fig. 2a). Interestingly, the highly divergent environmental
228 lineages encode the highly divergent TcdB subtypes B10 and B11 (C-I) and B12 (C-II) (Fig. 2a,
229 Table S2). This is consistent with an early divergence of B10-B12 in *C. difficile* evolution,
230 predating the emergence of TcdB subtypes found in the other clinical strains.
231
232 Interestingly, we also observed rare lateral transfer events involving only one of the two toxin
233 genes to create hybrid strains containing new subtype combinations. Examples include the
234 spontaneous emergence of an A1/<u>B4</u> strain within clade 1, and the emergence of an <u>A1</u>/B2 strain
235 in clade 2 (Fig. 2a). Thus, through lateral transfer and homologous recombination, subtype B4 has
236 likely replaced B1 in a clade 1 strain, and subtype A1 has likely replaced A2 in a clade 2 strain.
237 Furthermore, we observed many independent clades containing *tcdA*-/*tcdB*- *C. difficile* strains
238 (e.g., see six lineages marked by asterisks in Fig. 2a). This is consistent with previously reported
239 "defective" toxin clades[46], and indicates numerous independent losses of the pathogenicity locus
240 throughout *C. difficile* evolution.
241
242
243 ***Toxin subtyping of an independent dataset of clinical C. difficile isolates***
244

245 As an independent test dataset for our toxin subtyping method, we examined 351 genomes of *C.*
246 *difficile* isolates derived from a clinical cohort from Brigham and Women's Hospital (BWH) in
247 Boston (Fig. 2c)[47]. As they were not included in our initial database, they are ideal for testing the
248 robustness and effectiveness of our subtype classification. All identified toxins could be accurately
249 assigned to our reference sequences, with most (97%) aligning with 100% identity to our database,
250 and the remainder aligning with >= 99.8% identity. Out of 351 total strains, 62 (17.7%) were toxin
251 deficient, while 289 (82.3%) contained TcdA and/or TcdB genes (Table S4). Of these, there were
252 12 distinct subtype combinations, with frequencies similar to those observed in the NCBI dataset.
253 A1/B1 strains were most common (N = 222), followed by A2/B2 (N = 24), -/B4 (N = 11), and
254 A3/B3 (N = 10) (Fig. 2c). Therefore, our method was able to rapidly and automatically classify a
255 large dataset of 351 clinically relevant *C. difficile* isolates, with all sequences represented in our
256 current classification.
257
258
259 ***Intragenic recombination drives TcdB diversification***
260
261 We next focused on understanding the evolution of TcdA and TcdB variants and mechanisms for
262 their diversification. To visualize global patterns of variation within TcdA and TcdB, we
263 developed a haplotype coloring algorithm (https://github.com/doxeylab/haploColor) based on
264 previous methods for genome visualization[48] First, sequences are painted black where they
265 matched the reference sequence (i.e., B1.1). Then, remaining positions were painted different
266 colors where they matched selected other subtypes (Fig. 3a): blue when matching B3.1, gold when
267 matching B6.1, and green when matching TcsL. The result of this algorithm applied to the TcdB
268 alignment revealed a striking block-like and highly mosaic pattern of amino acid variation, which
269 strongly indicates recombination between subtypes (Fig. 3a). B1, B3, and B5 are composed of a
270 B1-like variation (black) pattern across their full-length sequences, while B6 and B7 are composed
271 of a B6-like pattern (gold) across their full-length sequences. B2, B4, B8, and B9, however, possess
272 a mosaic combination of B1-like and B6-like patterns. B4, B6, B7, and B8 share a distinct B6-like
273 pattern of amino acid variation across their N-terminal region including the GTD and CPD
274 domains, but when examining the DRBD, the B6-like pattern is shared by a different set of
275 subtypes (B2, B6, B7, B10, and B11). These patterns indicate ancestral within-gene ("intragenic")

276 recombination events involving distinct regions of TcdB. As a statistical test of recombination, we
277 further performed phylogenetic network analysis using SplitsTree[49]. Consistent with patterns of
278 amino acid variation and per-domain phylogenetic analysis, network analysis revealed significant
279 evidence of recombination within TcdB (p = 0; Phi test for recombination) (Fig. S4). In contrast
280 to TcdB, TcdA (1-1874) produced homogeneous patterns of variation across each subtype (Fig.
281 S5) and did not display evidence of recombination in network analysis (p = 0.186) (Fig. S4),
282 indicating that recombination occurs frequently only in TcdB, but not in TcdA.
283
284 We further performed separate phylogenetic analyses of each domain (GTD, CPD, DRBD, and
285 CROP) of TcdB (Fig. 3b). The phylogenetic tree of each domain produced two main groups
286 (labeled i and ii), which correspond with the B1-like and B6-like patterns revealed in the alignment
287 visualization (Fig. 3a). Each subtype can therefore be described as a chimeric combination of type
288 "i" (B1-like) or type "ii" (B6-like) domains (Fig. 3c). Based on the per-domain phylogenetic
289 relationships and recombination patterns, we formulated a potential evolutionary model for the
290 origin of TcdB subtypes (Fig. 3d). An early TcdB ancestor split into two main groups: (i) B1, B5,
291 and B3; and (ii) B6 and B7. Subtype B2 likely originated by a recombination event fusing an
292 ancestral type i and type ii toxin. B9 likely originated from a recombination event between B1 and
293 B2, B4 from a recombination event between B1 and a type ii toxin, and B8 from a recombination
294 event between B3 and a type ii toxin. Subtypes B10-B12, which are rare variants recently
295 identified, are early diverging lineages since they consistently outgrouped other subtypes in
296 phylogenetic analysis (Fig. 3b), consistent with their divergent lineages among other strains (Fig.
297 2a).
298
299 In addition to these major ancestral recombination events, we also identified a considerable degree
300 of "microrecombination" events involving exchange of small segments between subtypes. For
301 example, a single TcdB sequence (B1.59) from subtype B1 has acquired an N-terminal segment
302 that is clearly derived from subtype B2 or B9 (Fig. 3a**,** Figure S6). This unique TcdB gene, which
303 appears to be the result of a spontaneous recombination event between a B1 and B2-containing
304 strain, is derived from a newly assembled clinical isolate from a Fidaxomicin clinical trial
305 (SRS1378602). A second similar example is B1.58 from a clinical isolate (ECDC-040,
306 SRS1486176), which has acquired a DRBD and CROPS segment from a B2-containing strain

307 (Figure S6). Fourteen such cases of microrecombination including these are depicted in Figure S6.
308 TcdB in particular appears to have diversified through an extensive degree of intragenic
309 recombination involving both large and small segments.
310
311
312 ***Subtyping partitions TcdB into distinct functional and antigenic groups***
313
314 The value of subtyping classification is to facilitate a molecular understanding of the impact of
315 sequence variations on function and antigenicity. For instance, our sequence alignment divides the
316 GTD into two groups: one contains B4, B6, B7, and B8; and the rest form another group (Fig. 3b,
317 Fig. S7). Previous studies have reported two types of cell-rounding effects: TcdB1 and B2 are
318 known to induce rounded cells with many protrusions remaining attached to cell culture plate,
319 whereas TcdB from the strain 1470 and 8864 have been reported to cause rounded cells without
320 protrusions, which is similar to TcsL[50]. It has been proposed that this is a result of the altered
321 specificity of their GTD in targeting different small GTPases[32,50]. TcdB in strain 1470 is classified
322 as B4, and the strain 8864 expresses B7, thus our classification predicts that the group containing
323 B4/6/7/8 induces TcsL-like cell rounding phenotype. This is indeed the case for two recently
324 reported clinical strains HSJD-312 and HMX152: both express toxins classified as B6 under our
325 subtyping system (Table S2) and have been reported to induce TcsL-like cell rounding[51].
326
327 Another well-characterized functional motif in TcdB is its FZD-binding interface, with key
328 residues clearly defined by the co-crystal structure[37,38]. It has been reported that B2 lost the ability
329 to bind FZDs due to residue variations at FZD-binding interfaces[35,39,40]. To survey whether these
330 variations may also exist in other subtypes, we aligned the key residues across all TcdB sequences
331 and visualized them in color. As shown in Fig. 4a, FZD-binding motif is highly conserved across
332 B1/3/4/5/8/9, while B2/6/7/10 share the same set of residue changes. Thus, B6/7/10 are predicted
333 to lose FZD-binding capability similar to B2. B11 contains a subset of residue changes found in
334 B2 within this region and likely also has reduced binding to FZDs. This pattern is consistent with
335 the phylogenic alignment of the DRBD domain, in which B1/3/4/5/8/9 form group i and
336 B2/6/7/10/11 form the group ii (Fig. 3b, 3c). Interestingly, although most B2 variants possess FZD-
337 binding site substitutions, there are a few exceptions that contain a largely in-tact FZD binding

338 site. In particular, B2.12 assembled from strain 2007223 (ERS001491) contains only a single
339 amino acid substitution (F1597S) in this region. Examination of the alignment reveals that this is
340 likely due to a microrecombination event that has replaced most of the FZD binding site with a
341 B1-like segment (Fig. 4a, Fig. S6). A similar scenario occurred in a member of subtype B6, in
342 which a B1-like segment has partially replaced this region (Fig. S6).
343
344 Sequence variations between subtypes could also have a drastic impact on efficacy of therapeutic
345 antibodies and vaccines. Bezlotoxumab from Merck is the only monoclonal antibody against TcdB
346 that was approved by the FDA and is currently used to reduce the recurrence of CDI[52]. This
347 antibody was generated using fragments of TcdB1 as antigens and its epitope sites (located at the
348 N-terminal of CROPs) have been established through crystallography[53]. We thus aligned all key
349 residues within its epitope across all TcdB sequences, which revealed extensive residue changes
350 largely conserved in B2/6/7/9/10/11 (Fig. 4a). This is consistent with our alignment of the CROPs
351 domain that group B2/6/7/9/10/11 together (Fig. 3b, 3c). It has been shown that bezlotoxumab
352 exhibited as low as over ~700-fold reduction in neutralization efficacy against TcdB from several
353 RT027 strains, which likely express B2, compared with its efficacy against B1 from VPI10463[36].
354 It also showed a similarly low efficacy against a strain 8864, which expresses B7. These results
355 indicate that bezlotoxumab does not have good efficacy against CDI caused by strains that express
356 B2/6/7/9/10/11. Furthermore, there are also a few amino acid changes within the epitope region in
357 B3/B8, and it has been shown that bezlotoxumab has ~60-fold reduction in efficacy against the
358 TcdB from a RT078 strain[36], which likely express B3 (Table S1). These results clearly indicate
359 that subtype classification of toxins will be able to guide the use of bezlotoxumab in clinic.
360
361 In addition to bezlotoxumab, we also examined another monoclonal antibody PA41, which is
362 under development[36], and a single-domain antibody (also known as VHH or nanobody) E3[54]. The
363 epitopes for both have been well established through co-crystal structures[54,55]. Both recognize the
364 GTD domain, with E3 recognizing the N-terminus of TcdB (Fig. 4a). The epitope site for PA41 is
365 highly conserved across most subtypes except a single residue change (Y323H) in B4. This is
366 consistent with the previous finding that PA41 can potently neutralize TcdB from many different
367 strains except RT017 strains, which express B4[36]. The epitope site for E3 is conserved in most

368 subtypes except a single residue change (I58T or A) in B4/6/7/8/10/11/12, and the impact of this
369 single residue change remains to be examined experimentally.
370
371 We finally mapped evolutionary conservation across all available TcdB sequences onto the
372 recently reported crystal structure of TcdB[54] (Fig. 4b). Relative to the reference TcdB1 sequence,
373 amino acid variants are common across the full-length TcdB sequence and occur throughout each
374 domain (Fig. 4a) but some regions (e.g., N-terminus of the GTD, C-terminus of CROPS domain,
375 segments of the pore-forming region of the DRBD and C-terminus of the CROPS domain) were
376 highly conserved. Based on structure, we identified eight conserved surface patches containing
377 universally conserved residues which represent potential key therapeutic targets for developing
378 broad-spectrum diagnostics, antibodies, and vaccines (Fig. 4b).
379
380
381 ***Diff-base: a central hub for storing and analyzing TcdA and TcdB sequences***
382 To address the needs of the research and clinical community in understanding toxin subtyping and
383 variations, we developed an online open database freely accessible at *diffbase.uwaterloo.ca*.
384 DiffBase stores all unique TcdA and TcdB sequences identified to date from the NCBI and SRA
385 and organizes sequences into our subtype classification scheme. Different subtypes and individual
386 sequences can be explored and visualized in reference trees, with additional information such as
387 source strains, and links to other resources (Fig. S8). In addition, users can query their own TcdA
388 or TcdB sequences against the database using a built-in BLAST interface, which will report the
389 top matching sequences in the database and provide toxin classifications and other related
390 information. To keep up with new sequences and information concerning TcdA and TcdB,
391 DiffBase facilitates community feedback and allows users to submit new information to be added
392 to the next iteration of the database.
393

394 **Discussion**

395 Here we created the largest database to date capturing available TcdA and TcdB sequence
396 diversity. This up-to-date collection includes genes from sequenced *C. difficile* isolates in
397 GenBank, as well as thousands of genomes that were assembled, annotated and analyzed from the
398 NCBI short-read archive. We clustered TcdA and TcdB variants into phylogenetic subtypes, which
399 provided a robust classification that is both congruent with *C. difficile* genome phylogeny as well
400 as variation in functional and therapeutically relevant amino acids including TcdB regions targeted
401 by existing monoclonal antibodies. Our analysis revealed that TcdB undergoes extensive
402 homologous recombination, and its potential evolutionary history is proposed based on
403 recombination among various subtypes. Finally, our analysis revealed mapped eight conserved
404 patches across the TcdB structure, which will facilitate future studies that aim to develop
405 "universal" *C. difficile* therapeutics that broadly target all TcdB subtypes.

406

407 In general, there is some agreement between previously defined toxinotypes and our toxin
408 subtypes, but subtyping provides additional information as it is able to describe TcdA and TcdB
409 separately. For example, toxinotype 0 associates largely with the A1/B1 subtype, toxinotype III
410 associates largely with A2/B2, toxinotype IV with A3/B5, toxinotype VIII associates with -/B4,
411 toxinotype IX associates largely with A2/B6, toxinotype X associates with -/B7, and so on (Table
412 S1). However, subtype A3/B3 associated with toxinotypes V, VI, VII, XVI, XXVIII, all of which
413 are found in clade 5 strains. Moving forward, with improved abilities to perform genome
414 sequencing of clinical isolates, it will be increasingly possible to classify strains based on their
415 genome-wide phylogenetic relationships as well as their toxin subtypes.

416

417 In comparison to TcdA, our analysis identified a much greater degree of sequence variation within
418 TcdB and a larger number of subtypes. Given that we see evidence for extreme recombination in
419 TcdB but not TcdA, it is possible that there is a greater selective pressure for positive selection
420 and diversification of TcdB. We speculate that intragenic recombination of TcdB may drive
421 antigenic diversification, whereas in TcdA this process may be driven by truncation and variation
422 of its C-terminal CROPS region. The CROPs domain showed similarity with carbohydrate-binding
423 proteins and may contribute to toxin attachment to cells by binding to carbohydrate moieties (27,
424 42, 44). The CROPs domain may also act as a chaperone that protects other domains (45). Possibly

425 due to its repetitive nature, the CROPs domain is often the region that induces strong immune
426 responses. It remains to be determined whether frequent recombinations/changes in TcdA-CROPs
427 may alter its function and/or antigenicity.
428
429 These findings further suggest that TcdB may play a central role in *C. difficile* pathogenesis, which
430 is consistent with previous findings that TcdA-/TcdB+ mutant *C. difficile* strains are fully virulent,
431 whereas TcdA+/TcdB- strains are attenuated in multiple mouse models[26,56]. It has also been
432 suggested that TcdB is the primary factor for inducing the host immune and inflammatory
433 responses in mouse models[26]. The key role of TcdB in CDI is further confirmed by the findings
434 that an antibody that neutralizes TcdB (bezlotoxumab), but not another one that neutralizes TcdA
435 (actoxumab, Merck), conferred protection against CDI in gnotobiotic piglets [57] and reduced CDI
436 recurrence in humans[52,58] and it is also consistent with the fact that many clinical isolates only
437 express TcdB[59]. An exception to a dominant role for TcdB is the very rare TcdA+ TcdB- strain. It
438 is noteworthy that one such strain identified in GenBank contains the single most divergent TcdA
439 sequence (subtype A7)[45], which may have diverged to acquire a pathogenic functionality without
440 requiring TcdB.
441
442 For such recombination events to have occurred in TcdB, phylogenetically distinct *C. difficile*
443 strains containing different toxin subtypes must have coexisted within the same host individuals,
444 exchanged genetic material and recombined to produce new recombinant forms. Co-infection with
445 different *C. difficile* ribotypes has been recently reported in a clinical case study[60]. Theoretically,
446 co-infection does not need to occur frequently to promote recombination. A single individual
447 containing two or more *C. difficile* strains, may be sufficient to promote recombination, generating
448 hybrid toxins with different regions derived from different sequences or subtypes. The new
449 recombinant strain can then increase in frequency through transmission to other individuals. Our
450 analysis suggests that this process has not only occurred frequently in the past as a mechanism by
451 which different subtypes originated, but that it may be a frequent and ongoing process in new
452 clinical isolates (e.g., B1.59 from SRS1378602). Consideration of intragenic recombination and
453 how it may shape TcdB function and toxicity will be important in efforts to understand the
454 emergence of new *C. difficile* hypervirulent strains and develop targeted therapeutic interventions.
455

456 Recombination offers considerable adaptive benefits to proteins by facilitating rapid mutation of
457 a sequence by exchange of entire segments as opposed to the relatively slower process of single
458 point mutations. In this way, proteins can diversify by shuffling a few basic building blocks such
459 as protein domains. In pathogens, recombination plays a major role in pathoadaptive evolution by
460 facilitating rapid "switching" of virulence factors and antigenic proteins[61,62]. Antigenic
461 recombination can promote the sudden avoidance of immune recognition (antigenic escape),
462 which has been demonstrated for the *C. difficile* S-layer gene[63]. In the case of TcdB, intragenic
463 recombination may generate new hybrid toxins composed of different domains types and
464 functions. In theory, recombination could also generate resistance to therapeutics by replacing
465 entire binding interfaces with compatible regions from other toxins that possess drug-resistant
466 mutations. Recombination-mediated domain shuffling not only describes TcdB sequence patterns
467 and phylogenetic relationships, and also provides an explanation for important functional
468 differences between TcdB variants. For example, the exchange of a B6-like GTD between
469 subtypes B4, B8, B6, and B7, correlates with the TcsL-like clumping and rounding phenotype.
470 Also intriguing are the many microrecombination events that have occurred in the DRDB region
471 which overlap with FZD-binding site. For example, likely due to partial homologous
472 recombination with a B1-like toxin, one B2 variant (B2.12, strain 2007223 from ERS001491)
473 contains an in-tact FZD-binding interface with only a single amino acid substitution (F1597S).
474 This suggests that intragenic recombination in TcdB may promote rapid evolutionary switching
475 between receptor-binding activities or affinities.
476
477 Given the extent of TcdB diversification and its primary role in virulence, it is critically important
478 to identify conserved regions that can be targeted for therapeutic and diagnostic applications.
479 Sequence conservation mapped to protein structure also revealed at least 8 distinct surface patches
480 containing a high density of universally conserved residues across all TcdB subtypes, which
481 represent promising regions for the development of inhibitors. Importantly, the binding site for the
482 antibody therapeutic bezlotoxumab, which is commonly used to treat *C. difficile* infections, was
483 not among these and instead displayed considerable variation across TcdB subtypes with B2, B10,
484 B11, B9, B6, and B7 in particular displaying 7-8 likely destabilizing substitutions. Although the
485 common B1 subtype of TcdB is largely conserved across this region, based on analysis, it is
486 possible that intragenic recombination with other strains (e.g., a B2-containing strain) could

487 generate spontaneous resistance to bezlotoxumab by replacing this region with a B2-like segment.
488 Future efforts to target highly conserved clusters of surface-exposed residues on the TcdB structure
489 may yield promising candidates for therapeutic or vaccine development.
490
491 Finally, based on sequence-based classification of *tcdA* and *tcdB* genes, we propose a revised
492 scheme for naming these genes in future studies. In this scheme, a newly identified TcdA or TcdB
493 sequence may be aligned to our reference database and named based on the top hit according to
494 sequence identity, provided that the sequence exceeds thresholds used for our clustering (99.4%
495 for TcdA and 97.0% for TcdB). In order to enable automated subtyping of new *tcdA* and *tcdB*
496 genes and facilitate community collaboration and data sharing, we have developed a freely
497 available, online database (DiffBase) for use by *C. difficile* clinical and research community. In
498 the future, clinicians will be able to query toxin sequences from clinical isolates and immediately
499 determine the toxin subtype, which will help them decide on therapeutic strategies. For instance,
500 among the 351 clinical cases in the BWH dataset, there are 34 cases expressing B2/B6/B7/B9, for
501 which treatment of bezlotoxumab would not be effective. Therefore, toxin subtyping will guide
502 proper choices of clinical treatment in consideration of toxin variations and allow researchers to
503 monitor the ongoing evolution and diversification of *C. difficile*.
504
505

506 **Methods**

507

508 **Dataset construction**

509 *Assembly of 6492 C. difficile genomes from the NCBI short read archive*

510 A set of *Clostridiodes difficile* sequencing runs was retrieved from the NCBI short read archive
511 (SRA) by text query for "*Clostridioides difficile*" on June 20th, 2019. Metagenomic samples were
512 omitted, leaving only genomic samples to reduce the chance of contamination from other bacterial
513 species. Sequencing runs were downloaded using the fasterq-dump module of the SRA toolkit. To
514 account for multiple library preparation methods and adapters, the fastp tool[64] was used to perform
515 adapter trimming and quality control of the sequencing reads. For each quality-controlled set of
516 reads, SPAdes version 3.12[65] was used for genomes assembly, with *C. difficile* str. 630 as a
517 conservative reference and the --untrusted-contigs and --careful options. Each assembly was
518 automatically annotated using the Prokka pipeline[66] with a minimum contig length of 200. In order
519 to verify the identity of the assembled genomes as strains of *C. difficile,* the predicted genes from
520 Prokka were taxonomically annotated using Centrifuge[67] against their pre-compiled index of
521 bacterial, archaeal, viral, and human genomes. Only samples that were statistically verified as
522 belong to strains of *C. difficile* were kept.

523

524 To identify the *tcdA* and *tcdB* genes from all strains, the phmmer tool was used to search for
525 matches to TcdA (uniprot accession # Q189K5_CLOD6) and TcdB (uniport accession #
526 Q189K3_CLOD6) as queries. In order to distinguish true sequence variants from poorly
527 assembled, low-quality, or chimeric variants, only hits that clearly represented well-assembled
528 toxin sequences (that is, yielding a protein equal to or greater than 1,800 amino acids) were
529 retained. Sequences with apparent N- or C-terminal truncations representing less than 1% of the
530 total assembled data set were also removed. In total, the final re-assembled set of redundant TcdA
531 and TcdB sequences consisted of 3,542 and 5,994 sequences, respectively. Redundancy in each of
532 these sets was removed by clustering with CD-HIT version 4.6[68] at 100% identity. Non-redundant
533 sets were aligned using the L-INS-i algorithm of the MAFFT package[69].

534

535 *TcdA and TcdB sequences from the NCBI GenBank database and manually curated set*

536 GenBank homologs of TcdA and TcdB were also identified via a BLAST search of the NCBI non-
537 redundant database on Feb 8, 2020. TcdB and TcdA sequences from *C. difficile* strain 630 were
538 used as queries. Homologs were filtered to those with *E*-value < 1e-10, 70% identity and query
539 alignment coverage, which removed partial sequences. In addition, we manually curated 63
540 reference *C. difficile* strains collected from previous studies[12,41]. For these 63 genomes, we
541 manually identified corresponding strains within the NCBI or SRA database and identified *tcdA*
542 and *tcdB* genes based on pre-computed genome annotations or through similarity searches.
543 Fourteen genomes could not be associated with *tcdA* and *tcdB* genes in the NCBI; for these cases,
544 raw genomic reads were retrieved from European Nucleotide Archive (ENA) and were assembled
545 using SPADES as described earlier.
546
547 *Construction of TcdA and TcdB alignments*
548 A combined dataset of TcdA and TcdB homologs was created by pooling SRA-derived, NCBI-nr
549 derived, and the manually curated set of sequences. The combined set of sequences were aligned
550 using MUSCLE[70] with default parameters as implemented in Seaview[71]. Due to significant length
551 variation at the C-terminus of TcdA alignment, only the CROP-less core region (1-1874) of the
552 alignment was kept for subsequent analysis; while the entire TcdB alignment (1-2366) was used.
553 Redundant sequences (100% identity) were removed as well as sequences annotated as partial that
554 contained truncations in the alignment.
555
556 ***Sequence clustering and analysis***
557 TcdA and TcdB alignments were then processed separately using an analysis pipeline
558 implemented within R. For each case, the multiple sequence alignment was converted to a distance
559 matrix using the dist.alignment() function from the seqinr package[72]. Average linkage hierarchical
560 clustering was performed using the hclust() function. Pairwise sequence similarities were mapped
561 onto the clustering tree and visualized using the ComplexHeatmap package[73] and clustering
562 threshold were chosen to generate subtypes with strong internal (within-cluster) and lower external
563 (between-cluster) similarities based on visual analysis and quantitative analysis of percentage
564 identity distributions.
565

566 For analysis of amino acid variation, we converted the alignments into data matrices using the
567 alignment2matrix() function from the BALCONY R package[74]. We then identified all variant
568 residues across all alignment positions relative to the sequences of TcdA and TcdB from strain
569 630 as a reference. Residues implicated in frizzled binding[37], bezlotoxumab binding[53], PA41
570 binding[55], and E3 binding[54] were then analyzed in terms of their variation across subtypes. E3
571 binding residues were identified by analysis of PDB structure 6OQ5[54], by selecting atoms in chain
572 A (TcdB) within a 4 Å distance of chain E (E3) using PyMol's distance algebra functions. The
573 ComplexHeatmap R package was used for data visualization.
574
575 Analysis of repeats in TcdA was done using InterproScan as part of the InterPro 80.0 database[75].
576 The number of detected matches to ProSite's cell wall-binding repeat profile (PS51170) was
577 counted in the A1.1 reference sequence (UniProt P16154, 2710 aa), the longest (3070 aa) and
578 shortest (1889 aa) variants of TcdA in our database.
579
580 ***Structural analysis***
581 To map sequence conservation on to the structure of TcdB, we used the ConSurf server[76] with the
582 TcdB alignment as input and the recently determined crystal structure of full-length TcdB (PDB
583 ID 6OQ5)[54] as the template. Default parameters (neighbor-joining with ML distance and Bayesian
584 calculation of conservation scores) were used. Structural visualization was done using PyMol
585 version 2.3.4, using the recommended script (https://consurf.tau.ac.il/pyMOL/consurf_new.py)
586 with insufficient data hidden from the image.
587
588 ***Construction and toxin subtyping of C. difficile genome phylogeny***
589 We retrieved 2,118 assemblies for 1,934 representative *C. difficile* genomes
590 (https://www.ncbi.nlm.nih.gov/genome/tree/535) from the NCBI. The snippy pipeline
591 (https://github.com/tseemann/snippy) was used to map all genomes to the reference (strain 630,
592 GCA_000003215). For phylogenetic reconstruction, we analyzed 14,194 SNPs across 88
593 conserved marker genes (those present in *C. difficile*) derived from the PhyEco Firmicutes
594 dataset[77]. A phylogeny was reconstructed using RAXML with the GTRGAMMA model [78]. All
595 TcdA and TcdB homologs from the NCBI were then subtyped by BLAST against our database of
596 labeled toxin subtype sequences, using only the conserved portion (region 1-1874) of the TcdA

alignment, and the full 1-2366 regions from the TcdB alignments. An assignment script written in Perl was used to parse BLAST output files and assign subtypes. The subtype "X" associated with the best matching reference sequence (highest sequence identity) was assigned if the alignment coverage exceeded 90% and labeled as complete; otherwise, it was labeled as a partial sequence.

SplitsTree analysis of recombination

TcdA and TcdB alignments were analyzed by SplitsTree version 4.0[49]. A NeighborNet tree visualization was produced using protein maximum-likelihood distances according to the WAG model of evolution. The Phi test for recombination was performed as implemented in SplitsTree which selected a window size of 100 for TcdA with k = 3 and a window size of TcdB with k = 21.

Haplotype visualization

For visualization of recombinant blocks and haplotype structure within TcdA and TcdB protein alignments, we developed a modified algorithm based on a previous method from Wang et al.[48] for comparative genomic visualization. An implementation of this method in the R programming language is available at https://github.com/doxeylab/haploColor. The algorithms works as follows:

(1) Assign first sequence as reference.
(2) Assign all residues of reference a new color *C*.
(3) Assign positions in other sequences that match the reference, the same color *C*.
(4) Identify sequence most dissimilar to the current reference across unassigned positions, and assign it as the new reference.
(5) Repeat steps 2-3 for a defined number of iterations or until all sequences are completely colored.

The algorithm was applied directly to the TcdA and TcdB alignments and run for both 4 and 16 iterations (TcdB) and 16 iterations (TcdA).

Development of the DiffBase web-server

The DiffBase web server was developed as an R shiny() application. Contained within DiffBase is an implementation of BLAST+. Individual sequences can be submitted to the server, where the

628 blastp program is run to find matches from within the entirety of the server sequence repositories.
629 An *E*-value cutoff of 1e-10 is used to filter hits, and the results are sorted by percent identity
630 between query and target sequences. Toxin groups can also be viewed in a phylogenetic tree
631 visualized using ggtree R package[79]. Metadata about group members was obtained from the NCBI
632 Identical Protein Group (IPG) database. The source code is freely available at
633 https://github.com/doxeylab/diffBase.
634
635
636 **Data Availability**
637 Our open source online database is available at: https://diffbase.uwaterloo.ca and
638 https://github.com/doxeylab/diffbase.
639 All source code for analyses is available at: https://github.com/doxeylab/diffBaseAnalyses
640
641
642 **Acknowledgments**

643 A.C.D. acknowledges funding from the Natural Sciences and Engineering Research Council of
644 Canada (NSERC Discovery Grant, RGPIN-2019-04266; Discovery Accelerator Supplement,
645 RGPAS-2019-00004), and from the Government of Ontario (Early Researcher Award). A.C.D.
646 holds a University Research Chair at the University of Waterloo.
647
648 M.D. acknowledges support from National Institute of Health (NIH) (R01AI132387 and
649 R01AI139087 to M.D.), the NIH-funded Harvard Digestive Disease Center (P30DK034854), and
650 Boston Children's Hospital Intellectual and Developmental Disabilities Research Center
651 (P30HD18655). M.D. holds the Investigator in the Pathogenesis of Infectious Disease award from
652 the Burroughs Wellcome Fund.
653

654 J. W. acknowledges support from the Intramural Research Program of the National Library of
655 Medicine, NIH. L.B. acknowledges support from NIH (P30 DK034854), Hatch Family
656 Foundation, and Brigham and Women's Hospital Precision Medicine Institute.

657
658

659 **References**

660

661 1. Knight, D. R., Elliott, B., Chang, B. J., Perkins, T. T. & Riley, T. V. Diversity and
662 evolution in the genome of *Clostridium difficile*. *Clin. Microbiol. Rev.* **28**, 721–741
663 (2015).
664 2. Guh, A. Y. *et al.* Trends in U.S. burden of *Clostridioides difficile* infection and outcomes.
665 *N. Engl. J. Med.* **382**, 1320–1330 (2020).
666 3. Heinlen, L. & Ballard, J. D. *Clostridium difficile* infection. *Am. J. Med. Sci.* **340**, 247–252
667 (2010).
668 4. Rupnik, M., Wilcox, M. H. & Gerding, D. N. *Clostridium difficile* infection: New
669 developments in epidemiology and pathogenesis. *Nat. Rev. Microbiol.* **7**, 526–536 (2009).
670 5. Martin, J. S. H., Monaghan, T. M. & Wilcox, M. H. *Clostridium difficile* infection:
671 Epidemiology, diagnosis and understanding transmission. *Nat. Rev. Gastroenterol.*
672 *Hepatol.* **13**, 206–216 (2016).
673 6. Smits, W. K., Lyras, D., Lacy, D. B., Wilcox, M. H. & Kuijper, E. J. *Clostridium difficile*
674 infection. *Nat. Rev. Dis. Prim.* **2**, 16020 (2016).
675 7. Abt, M. C., McKenney, P. T. & Pamer, E. G. *Clostridium difficile* colitis: Pathogenesis
676 and host defence. *Nat. Rev. Microbiol.* **14**, 609–620 (2016).
677 8. Lessa, F. C. *et al.* Burden of *Clostridium difficile* infection in the United States. *N. Engl. J.*
678 *Med.* **372**, 825–834 (2015).
679 9. Knetsch, C. W. *et al.* Current application and future perspectives of molecular typing
680 methods to study clostridium difficile infections. *Eurosurveillance* **18**, 20381 (2013).
681 10. Griffiths, D. *et al.* Multilocus sequence typing of *Clostridium difficile*. *J. Clin. Microbiol.*
682 **48**, 770–8 (2010).
683 11. Eyre, D. W. *et al.* Diverse sources of *C. difficile* infection identified on whole-genome
684 sequencing. *N. Engl. J. Med.* **369**, 1195–1205 (2013).
685 12. Bletz, S., Janezic, S., Harmsen, D., Rupnik, M. & Mellmann, A. Defining and Evaluating
686 a Core Genome Multilocus Sequence Typing Scheme for Genome-Wide Typing of
687 *Clostridium difficile*. *J. Clin. Microbiol.* **56**, (2018).
688 13. Janezic, S. & Rupnik, M. Development and Implementation of Whole Genome
689 Sequencing-Based Typing Schemes for *Clostridioides difficile*. *Front. Public Heal.* **7**, 309

690 (2019).
691 14. Dingle, K. E. *et al.* Evolutionary history of the *Clostridium difficile* pathogenicity locus.
692 *Genome Biol. Evol.* **6**, 36–52 (2014).
693 15. Janezic, S., Potocnik, M., Zidaric, V. & Rupnik, M. Highly divergent *Clostridium difficile*
694 strains isolated from the environment. *PLoS One* **11**, e0167101 (2016).
695 16. He, M. *et al.* Evolutionary dynamics of *Clostridium difficile* over short and long time
696 scales. *Proc. Natl. Acad. Sci. U. S. A.* **107**, 7527–7532 (2010).
697 17. Collins, J. *et al.* Dietary trehalose enhances virulence of epidemic *Clostridium difficile*.
698 *Nature* **553**, 291–294 (2018).
699 18. He, M. *et al.* Emergence and global spread of epidemic healthcare-associated *Clostridium*
700 *difficile*. *Nat. Genet.* **45**, 109–113 (2013).
701 19. McDonald, L. C. *et al.* An epidemic, toxin gene-variant strain of *Clostridium difficile*. *N.*
702 *Engl. J. Med.* **353**, 2433–2441 (2005).
703 20. Loo, V. G. *et al.* A predominantly clonal multi-institutional outbreak of *Clostridium*
704 *difficile* - Associated diarrhea with high morbidity and mortality. *N. Engl. J. Med.* **353**,
705 2442–2449 (2005).
706 21. Goorhuis, A. *et al.* Emergence of *Clostridium difficile* infection due to a new
707 hypervirulent strain, polymerase chain reaction ribotype 078. *Clin. Infect. Dis.* **47**, 1162–
708 70 (2008).
709 22. Jhung, M. A. *et al.* Toxinotype V *Clostridium difficile* in humans and food animals.
710 *Emerg. Infect. Dis.* **14**, 1039–1045 (2008).
711 23. Collins, J., Danhof, H. & Britton, R. A. The role of trehalose in the global spread of
712 epidemic *Clostridium difficile*. *Gut Microbes* **10**, 204–209 (2019).
713 24. Aktories, K., Schwan, C. & Jank, T. *Clostridium difficile* Toxin Biology. *Annu. Rev.*
714 *Microbiol.* **71**, 281–307 (2017).
715 25. Voth, D. E. & Ballard, J. D. *Clostridium difficile* toxins: Mechanism of action and role in
716 disease. *Clin. Microbiol. Rev.* **18**, 247–263 (2005).
717 26. Carter, G. P. *et al.* Defining the Roles of TcdA and TcdB in Localized Gastrointestinal
718 Disease, Systemic Organ Damage, and the Host Response during *Clostridium difficile*
719 Infections. *MBio* **6**, e00551 (2015).
720 27. Pruitt, R. N. & Lacy, D. B. Toward a structural understanding of *Clostridium difficile*

721 toxins A and B. *Front. Cell. Infect. Microbiol.* **2**, 28 (2012).
722 28. Gerding, D. N., Sambol, S. P. & Johnson, S. Non-toxigenic clostridioides (formerly
723 clostridium) difficile for prevention of *C. difficile* infection: From bench to bedside back
724 to bench and back to bedside. *Front. Microbiol.* **9**, 1700 (2018).
725 29. Schirmer, J. & Aktories, K. Large clostridial cytotoxins: Cellular biology of Rho/Ras-
726 glucosylating toxins. *Biochim. Biophys. Acta - Gen. Subj.* **1673**, 66–74 (2004).
727 30. Jank, T. & Aktories, K. Structure and mode of action of clostridial glucosylating toxins:
728 the ABCD model. *Trends Microbiol.* **16**, 222–229 (2008).
729 31. Orrell, K. E., Mansfield, M. J., Doxey, A. C. & Melnyk, R. A. The *C. difficile* toxin B
730 membrane translocation machinery is an evolutionarily conserved protein delivery
731 apparatus. *Nat. Commun.* **11**, 432 (2020).
732 32. Genth, H. *et al.* Haemorrhagic toxin and lethal toxin from *Clostridium sordellii* strain
733 vpi9048: Molecular characterization and comparative analysis of substrate specificity of
734 the large clostridial glucosylating toxins. *Cell. Microbiol.* **16**, 1706–1721 (2014).
735 33. Davies, A. H., Roberts, A. K., Shone, C. C. & Acharya, K. R. Super toxins from a super
736 bug: structure and function of *Clostridium difficile* toxins. *Biochem. J.* **436**, 517–526
737 (2011).
738 34. Lanis, J. M., Heinlen, L. D., James, J. A. & Ballard, J. D. *Clostridium difficile*
739 027/BI/NAP1 encodes a hypertoxic and antigenically variable form of TcdB. *PLoS*
740 *Pathog.* **9**, e1003523 (2013).
741 35. Chung, S.-Y. *et al.* The Conserved Cys-2232 in *Clostridioides difficile* Toxin B Modulates
742 Receptor Binding. *Front. Microbiol.* **9**, 2314 (2018).
743 36. Marozsan, A. J. *et al.* Protection against *Clostridium difficile* infection with broadly
744 neutralizing antitoxin monoclonal antibodies. *J. Infect. Dis.* **206**, 706–713 (2012).
745 37. Chen, P. *et al.* Structural basis for recognition of frizzled proteins by *Clostridium difficile*
746 toxin B. *Science* **360**, 664–669 (2018).
747 38. Tao, L. *et al.* Frizzled proteins are colonic epithelial receptors for *C. difficile* toxin B.
748 *Nature* **538**, 350–355 (2016).
749 39. Peng, Z. *et al.* Designed Ankyrin Repeat Protein (DARPin) Neutralizers of TcdB from
750 *Clostridium difficile* Ribotype 027. *mSphere* **4**, e00596-19 (2019).
751 40. López-Ureña, D. *et al.* Toxin B Variants from *Clostridium difficile* Strains VPI 10463 and

752 NAP1/027 Share Similar Substrate Profile and Cellular Intoxication Kinetics but Use
753 Different Host Cell Entry Factors. *Toxins (Basel).* **11**, (2019).
754 41. M, R. & S, J. An Update on *Clostridium Difficile* Toxinotyping. *J. Clin. Microbiol.* **54**,
755 (2016).
756 42. Rupnik, M. Clostridium difficile toxinotyping. *Methods Mol. Biol.* **646**, 67–76 (2010).
757 43. Von Eichel-Streiber, C., Sauerborn, M. & Kuramitsu, H. K. Evidence for a modular
758 structure of the homologous repetitive C-terminal carbohydrate-binding sites of
759 *Clostridium difficile* toxins and *Streptococcus mutans* glucosyltransferases. *J. Bacteriol.*
760 **174**, 6707–6710 (1992).
761 44. von Eichel-Streiber, C., Laufenberg-Feldmann, R., Sartingen, S., Schulze, J. & Sauerborn,
762 M. Comparative sequence analysis of the *Clostridium difficile* toxins A and B. *MGG Mol.*
763 *Gen. Genet.* **233**, 260–268 (1992).
764 45. M, M. *et al.* Clostridium Difficile: New Insights Into the Evolution of the Pathogenicity
765 Locus. *Sci. Rep.* **5**, 15023 (2015).
766 46. Stabler, R. A. *et al.* Comparative phylogenomics of *Clostridium difficile* reveals clade
767 specificity and microevolution of hypervirulent strains. *J. Bacteriol.* **188**, 7297–305
768 (2006).
769 47. Worley, J. N. *et al.* Genomic determination of relative risks for *Clostridioides difficile*
770 infection from asymptomatic carriage in ICU patients. *Clin. Infect. Dis.* In Press. (2020).
771 doi:doi:10.1093/cid/ciaa894
772 48. Wang, J. R., de Villena, F. P.-M. & McMillan, L. Comparative analysis and visualization
773 of multiple collinear genomes. *BMC Bioinformatics* **13 Suppl 3**, S13 (2012).
774 49. Huson, D. H. SplitsTree: Analyzing and visualizing evolutionary data. *Bioinformatics*
775 (1998). doi:10.1093/bioinformatics/14.1.68
776 50. Chaves-Olarte, E. *et al.* R-Ras glucosylation and transient RhoA activation determine the
777 cytopathic effect produced by toxin B variants from toxin A-negative strains of
778 *Clostridium difficile*. *J. Biol. Chem.* **278**, 7956–7963 (2003).
779 51. Ramírez-Vargas, G. *et al.* Novel Clade C-I *Clostridium difficile* strains escape diagnostic
780 tests, differ in pathogenicity potential and carry toxins on extrachromosomal elements.
781 *Sci. Rep.* **8**, 13951 (2018).
782 52. Wilcox, M. H. *et al.* Bezlotoxumab for Prevention of Recurrent *Clostridium difficile*

783 Infection. *N. Engl. J. Med.* **376**, 305–317 (2017).
784 53. Orth, P. *et al.* Mechanism of action and epitopes of *Clostridium difficile* toxin B-
785 neutralizing antibody bezlotoxumab revealed by X-ray crystallography. *J. Biol. Chem.*
786 **289**, 18008–21 (2014).
787 54. Chen, P. *et al.* Structure of the full-length *Clostridium difficile* toxin B. *Nat. Struct. Mol.*
788 *Biol.* **26**, 712–719 (2019).
789 55. Kroh, H. K. *et al.* A neutralizing antibody that blocks delivery of the enzymatic cargo of
790 *Clostridium difficile* toxin TcdB into host cells. *J. Biol. Chem.* **293**, 941–952 (2018).
791 56. Lyras, D. *et al.* Toxin B is essential for virulence of *Clostridium difficile*. *Nature* **458**,
792 1176–1179 (2009).
793 57. Steele, J., Mukherjee, J., Parry, N. & Tzipori, S. Antibody against TcdB, but not TcdA,
794 prevents development of gastrointestinal and systemic *Clostridium difficile* disease. *J.*
795 *Infect. Dis.* **207**, 323–30 (2013).
796 58. Gupta, S. B. *et al.* Antibodies to Toxin B Are Protective Against *Clostridium difficile*
797 Infection Recurrence. *Clin. Infect. Dis.* **63**, 730–734 (2016).
798 59. Janezic, S., Marín, M., Martín, A. & Rupnika, M. A new type of toxin a-negative, toxin B-
799 positive *Clostridium difficile* strain lacking a complete tcdA gene. *J. Clin. Microbiol.* **53**,
800 692–695 (2015).
801 60. Wang, L. *et al.* Coinfection with 2 *Clostridium difficile* ribotypes in China. *Medicine*
802 *(Baltimore).* **97**, e9946 (2018).
803 61. Awadalla, P. The evolutionary genomics of pathogen recombination. *Nat. Rev. Genet.* **4**,
804 50–60 (2003).
805 62. Wilson, D. J. *et al.* Rapid evolution and the importance of recombination to the
806 gastroenteric pathogen *Campylobacter jejuni*. *Mol. Biol. Evol.* **26**, 385–397 (2009).
807 63. Dingle, K. E. *et al.* Recombinational switching of the *Clostridium difficile* S-layer and a
808 novel glycosylation gene cluster revealed by large-scale whole-genome sequencing. *J.*
809 *Infect. Dis.* **207**, 675–86 (2013).
810 64. Chen, S., Zhou, Y., Chen, Y. & Gu, J. fastp: an ultra-fast all-in-one FASTQ preprocessor.
811 *Bioinformatics* **34**, i884–i890 (2018).
812 65. Bankevich, A. *et al.* SPAdes: a new genome assembly algorithm and its applications to
813 single-cell sequencing. *J. Comput. Biol.* **19**, 455–77 (2012).

814 66. Seemann, T. Prokka: rapid prokaryotic genome annotation. *Bioinformatics* **30**, 2068–2069
815 (2014).
816 67. Kim, D., Song, L., Breitwieser, F. P. & Salzberg, S. L. Centrifuge: rapid and sensitive
817 classification of metagenomic sequences. *Genome Res.* **26**, 1721–1729 (2016).
818 68. Li, W. & Godzik, A. Cd-hit: a fast program for clustering and comparing large sets of
819 protein or nucleotide sequences. *Bioinformatics* **22**, 1658–1659 (2006).
820 69. Katoh, K. & Standley, D. M. MAFFT multiple sequence alignment software version 7:
821 improvements in performance and usability. *Mol. Biol. Evol.* **30**, 772–80 (2013).
822 70. Edgar, R. C. MUSCLE: multiple sequence alignment with high accuracy and high
823 throughput. *Nucleic Acids Res.* **32**, 1792–7 (2004).
824 71. Gouy, M., Guindon, S. & Gascuel, O. SeaView version 4: A multiplatform graphical user
825 interface for sequence alignment and phylogenetic tree building. *Mol. Biol. Evol.* **27**, 221–
826 4 (2010).
827 72. Charif, D. & Lobry, J. R. SeqinR 1.0-2: A Contributed Package to the R Project for
828 Statistical Computing Devoted to Biological Sequences Retrieval and Analysis. in 207–
829 232 (Springer, Berlin, Heidelberg, 2007). doi:10.1007/978-3-540-35306-5_10
830 73. Gu, Z., Eils, R. & Schlesner, M. Complex heatmaps reveal patterns and correlations in
831 multidimensional genomic data. *Bioinformatics* **32**, 2847–9 (2016).
832 74. Płuciennik, A. *et al.* BALCONY: an R package for MSA and functional compartments of
833 protein variability analysis. *BMC Bioinformatics* **19**, 300 (2018).
834 75. Hunter, S. *et al.* InterPro: The integrative protein signature database. *Nucleic Acids Res.*
835 **37**, (2009).
836 76. Ashkenazy, H. *et al.* ConSurf 2016: an improved methodology to estimate and visualize
837 evolutionary conservation in macromolecules. *Nucleic Acids Res.* **44**, W344-50 (2016).
838 77. Wu, D., Jospin, G. & Eisen, J. A. Systematic Identification of Gene Families for Use as
839 'Markers' for Phylogenetic and Phylogeny-Driven Ecological Studies of Bacteria and
840 Archaea and Their Major Subgroups. *PLoS One* (2013).
841 doi:10.1371/journal.pone.0077033
842 78. Stamatakis, A. RAxML version 8: a tool for phylogenetic analysis and post-analysis of
843 large phylogenies. *Bioinformatics* **30**, 1312–1313 (2014).
844 79. Yu, G., Smith, D. K., Zhu, H., Guan, Y. & Lam, T. T. ggtree : an r package for

visualization and annotation of phylogenetic trees with their covariates and other associated data. *Methods Ecol. Evol.* **8**, 28–36 (2017).

Figures and Tables

Table 1. Assembled *C. difficile* genomes from the NCBI SRA and associated statistics.

Property	**Statistic (mean +/- SD)**
Number of samples	6,492
Assembly length	4.2759 +/- 0.019 Mb
Number of contigs	403.6 +/- 544
GC content	28.33 +/- 4.14 % GC
Mean contig length	62.68 +/- 46.97 Kb
Contig N50	905,900.13 +/- 865,085
Contig N90	298,748 +/- 52,843.68

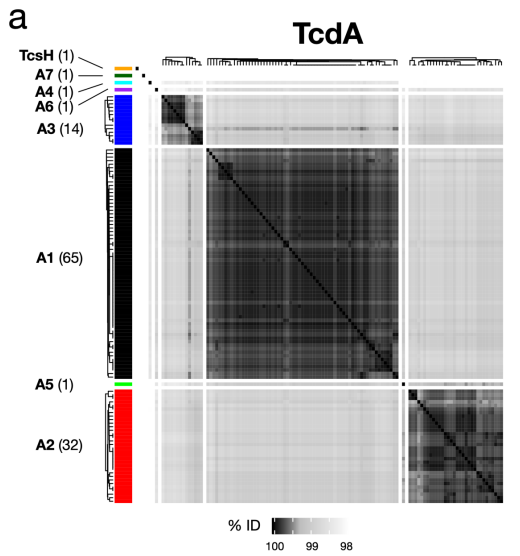

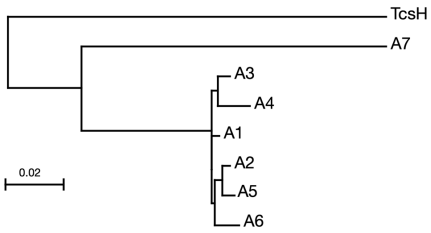

c

Subtype	A1	A2	A3	A4	A5	A6	A7	Rep. Strain
A1								VPI 10463
A2	99.0							R20291
A3	98.9	98.9						M120
A4	98.6	98.0	98.4					L;13.7548369.T
A5	99.1	99.4	98.5	97.9				ECDC-088
A6	98.9	98.6	98.2	97.6	98.5			ECDC-009
A7	85.6	85.5	85.6	84.6	85.3	85.3		RA09-70
TcsH	81.4	81.3	81.2	80.6	81.2	80.9	77.0	*P. sordellii*

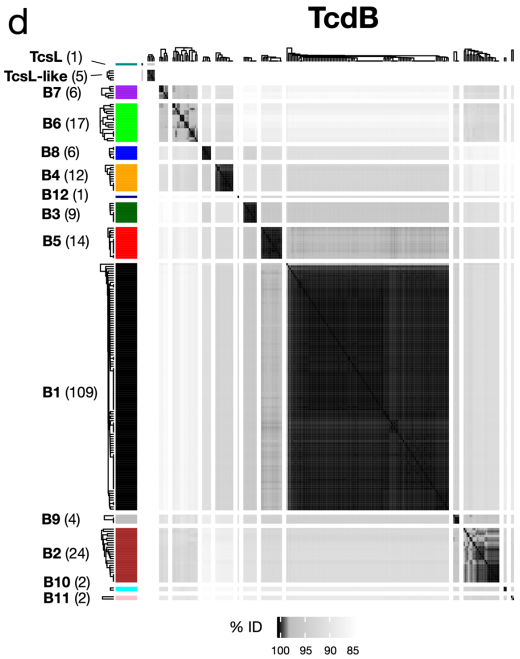

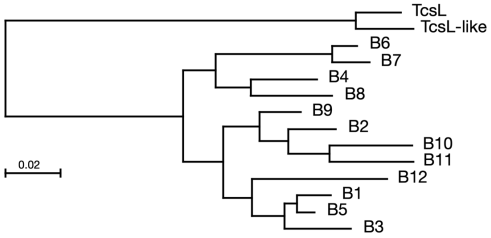

f

Subtype	B1	B2	B3	B4	B5	B6	B7	B8	B9	B10	B11	B12	TcsL	Rep. Strain
B1														VPI 10463
B2	92.2													R20291
B3	96.1	91.1												M120
B4	93.7	88.1	90.8											1470
B5	98.2	92.6	96.4	92.9										55767
B6	86.9	93.1	86.1	92.7	87.5									51680
B7	86.1	92.2	85.5	91.9	86.8	97.7								8864
B8	91.5	87.0	94.3	94.8	92.1	90.1	89.5							ES 130
B9	94.4	96.7	92.8	89.9	94.7	90.3	90.4	88.8						SE 844
B10	88.9	94.0	88.1	86.2	89.5	90.5	91.7	85.7	92.6					CD10-165
B11	89.4	93.7	88.4	86.6	89.9	90.2	89.6	85.7	92.1	94.1				CD160
B12	92.4	90.4	91.8	87.8	93.3	85.7	85.3	87.8	91.1	88.4	88.7			173070
TcsL	76.5	77.1	76.8	76.5	77.3	76.8	76.4	77.0	76.4	76.6	76.3	76.4		*P. sordellii*
TcsL-like	76.1	76.7	76.6	76.0	77.0	76.4	76.0	76.9	76.1	76.1	76.0	76.2	96.3	*P. sordellii*

Figure 1. Clustering of TcdA and TcdB sequences derived from NCBI GenBank and SRA into subtypes. (**a**) Hierarchical clustering of TcdA sequences, split into 8 groups. (**b**) Neighbor-joining phylogenetic tree of representative sequences of each TcdA subtype. (**c**) Percentage identities between representative sequences. (**d**) Hierarchical clustering of TcdB sequences, split into 14 groups. (**e**) Neighbor-joining phylogenetic tree of representative sequences of each TcdB subtype. (**f**) Percentage identities between representative sequences. Hierarchical clustering was performed using the hclust() function in R, and cluster definitions were selected based on strong within-cluster sequence similarities and weak between-cluster similarities, as demonstrated visually and quantitatively. The reference strains (VPI 10463 and strain 630) are associated with TcdA group A1 and TcdB group B1. The hypervirulent ribotype 027 strains such as R12087 and R20291 are associated with TcdA group A2 and TcdB group B2. Also included are the homologs of TcdA and TcdB (TcdH and TcdL, respectively) from *P. sordellii*, which expectedly exhibit the highest divergence from other groups. The datasets include TcdA and TcdB sequences from the NCBI GenBank as well as an additional 125 sequences assembled from the SRA.

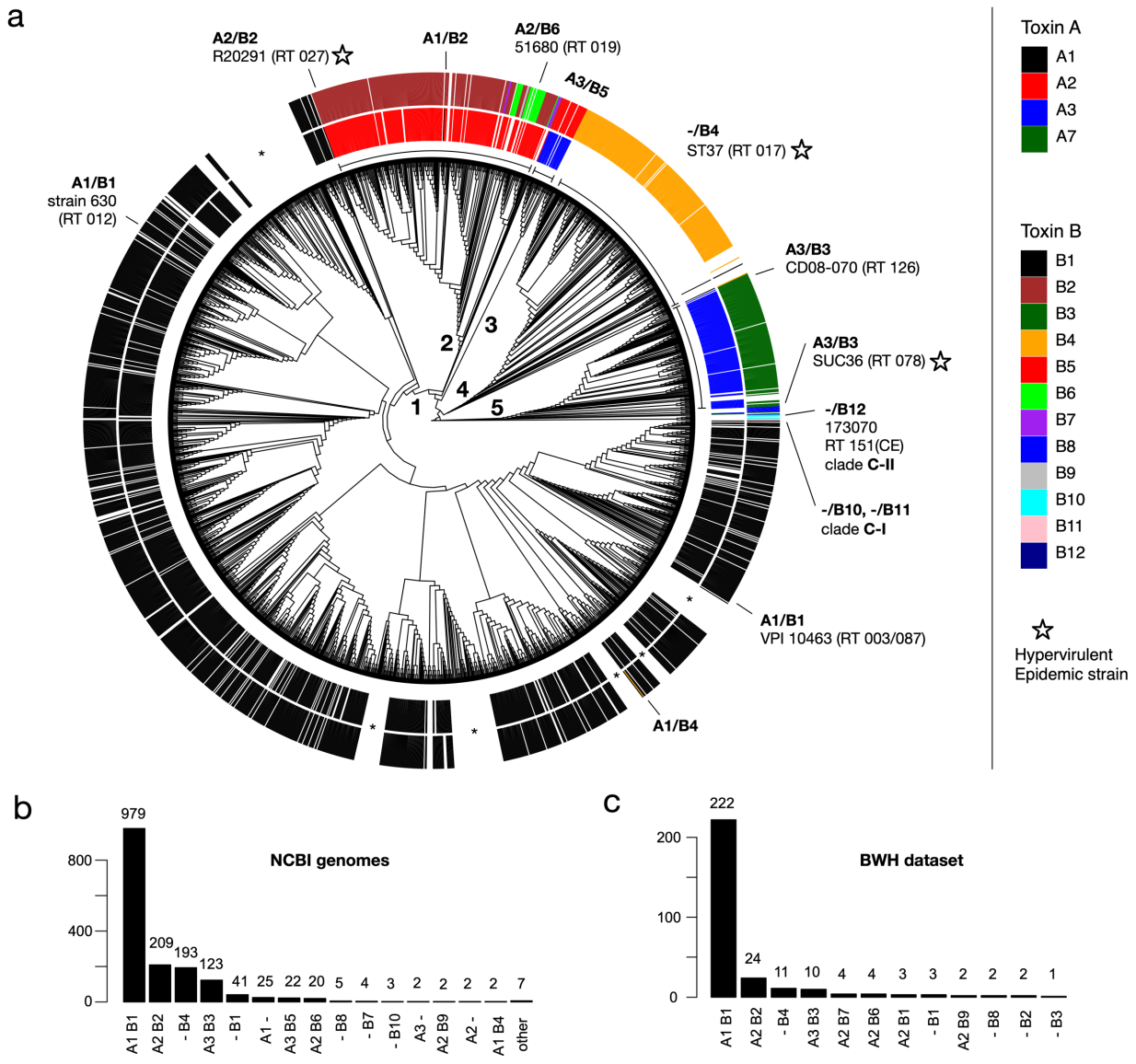

Figure 2. Toxin subtypes across the *C. difficile* phylogeny and occurrence of subtypes in a clinical CDI cohort. (**a**) TcdA (inner ring) and TcdB (outer ring) subtypes mapped onto a tree of 1934 *C. difficile* genomes. The genome tree is derived from the NCBI and is based on clustering of all-by-all genome BLAST scores. Lineages corresponding to previously identified *C. difficile* PaLoc clades (1 – 5) are labeled numerically. PaLoC clade 1 was subdivided into four sublineages labeled 1a-1d. Selected, clinically relevant strains are shown on the tree, with hypervirulent/epidemic outbreak strains indicated by stars. (**b**) Frequency of toxin subtypes detected in 1,934 representative, complete *C. difficile* genomes from NCBI/GenBank. A total of 1640 (84.8%) *C. difficile* strains contained TcdA and/or TcdB, while 294 (15.2%) were toxin deficient. (**c**) Frequency of toxin subtypes detected in a CDI clinical cohort from Brigham and Women's Hospital (BWH). The total dataset contained 351 *C. difficile* genomes derived from infected patients. Of these, 289 (82.3%) contained toxin genes, and 62 (17.7%) were toxin deficient.

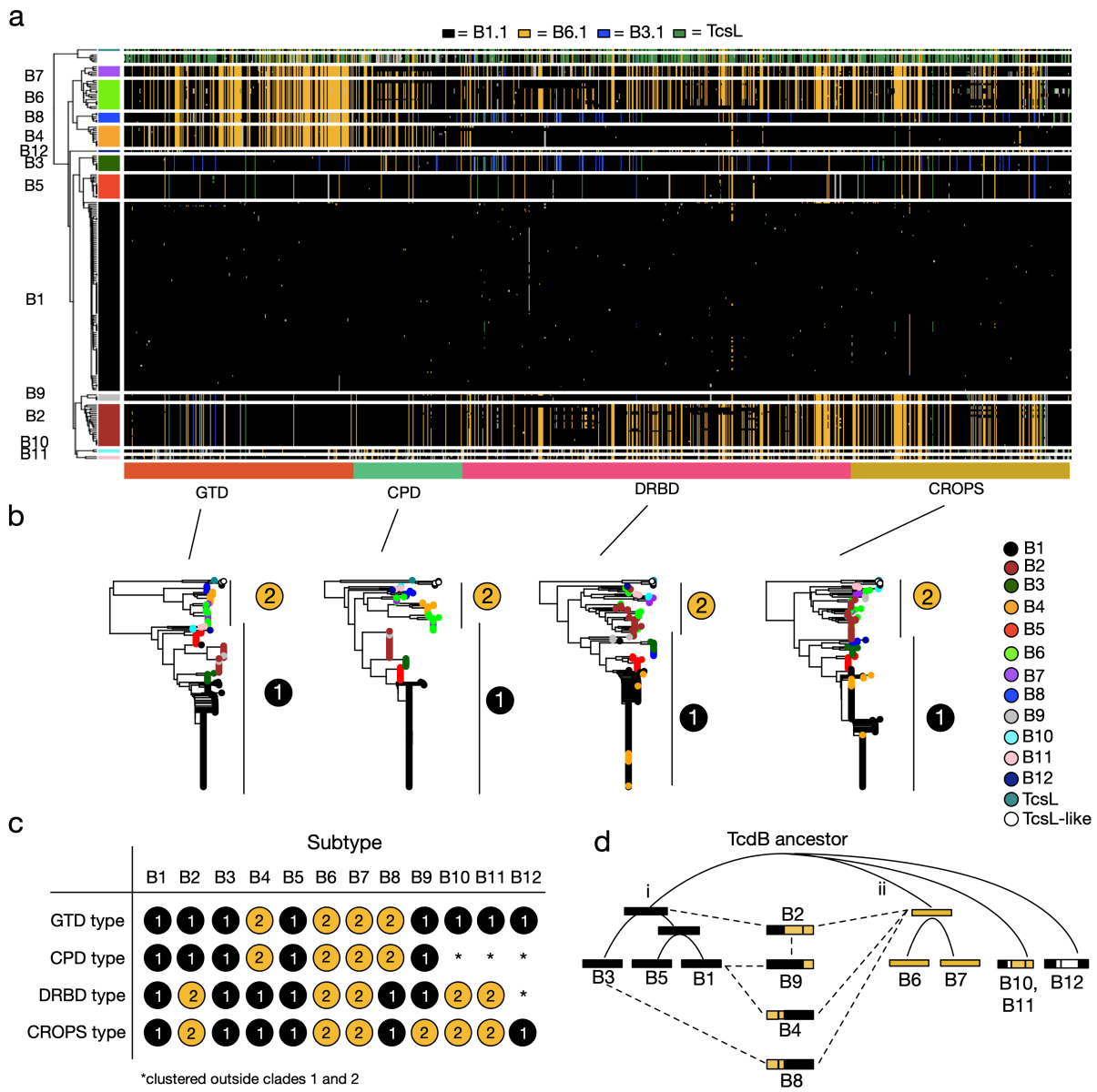

Figure 3. **Evolutionary diversification of TcdB by intragenic recombination and domain shuffling.** (**a**) Visualization of amino acid variation patterns in TcdB using a newly developed haplotype coloring algorithm (HaploColor). The visualization shows patterns of amino acid variation across the TcdB alignment. In this algorithm, the first sequence (B1.1) is assigned a distinct color, and all other sequences are colored the same color where they match this first sequence. Then, the process is repeated using a second sequence (B6.1) as the new reference, and so on. This reveals multiple colored segments indicative of common ancestry (identity by descent). Mosaic patterns are indicative of intragenic recombination. **(b)** Phylogenetic trees of TcdB based on individual domains. Each domain tree can be subdivided into two types (labeled 1 and 2), which allows each subtype to be described based on its domain composition (**c**). This reveals that TcdB subtypes are composed of domains with variable evolutionary histories, indicative of domain shuffling and intragenic recombination. (**d**) Evolutionary model depicting relationships between subtypes and putative recombination events. Here, TcdB split early into two main groups (i and ii). Subtype B2 likely originated by a recombination event fusing an ancestral type i and type ii toxin. B9 likely originated from recombination between B1 and B2, B4 from recombination between B1 and a type ii toxin, and B8 from recombination between B3 and a type ii toxin.

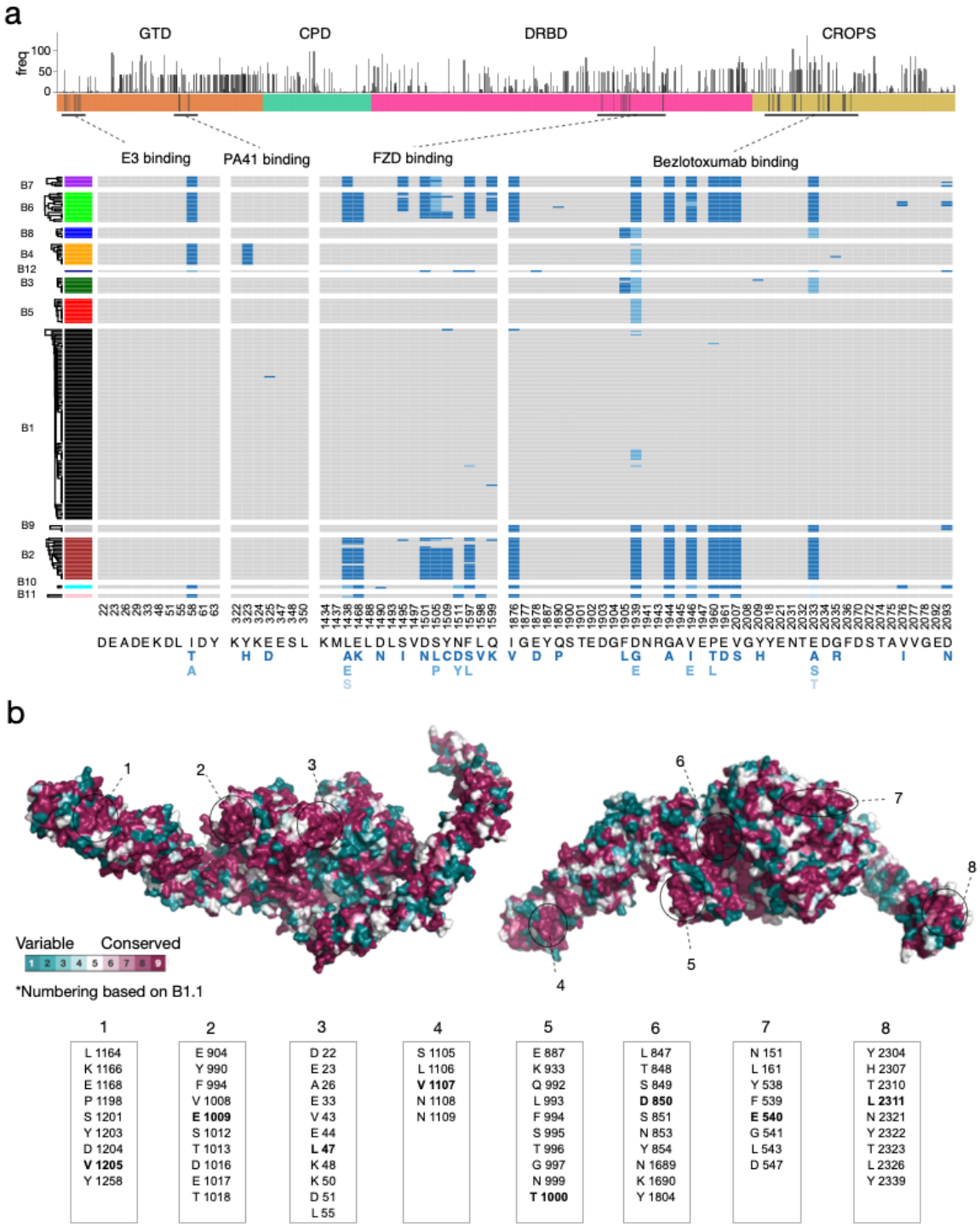

Figure 4. Conservation and functional variation across TcdB subtypes. (**a**) Frequency of amino acid variants across all positions of TcdB. The height of the bar indicates the number of unique TcdB sequences that contain a substitution relative to the classical TcdB1 (B1.1) sequence from strain 630 and VPI10463. Below this is a plot of amino acid variation for key functional regions including the binding sites for the frizzled receptor (FZD) and the antibodies (E3, PA41, and bezlotoxumab). The alignment is colored gray for residues that match the common amino acid found in B1.1, and variants are colored blue (darkest blue = most common variant). E3 and PA41 binding sites

are highly conserved, whereas FZD and bezlotoxumab binding sites are highly variable. FZD and bezlotoxumab variants also co-occur with each other. (**b**) Evolutionary conservation mapped to the protein structure of full length TcdB based on PDB 6OQ5[54]. Eight highly conserved surface patches are indicated, and additional details are in Fig. S7. Center residues within each surface patch are indicated in bold font.

Supplementary Data

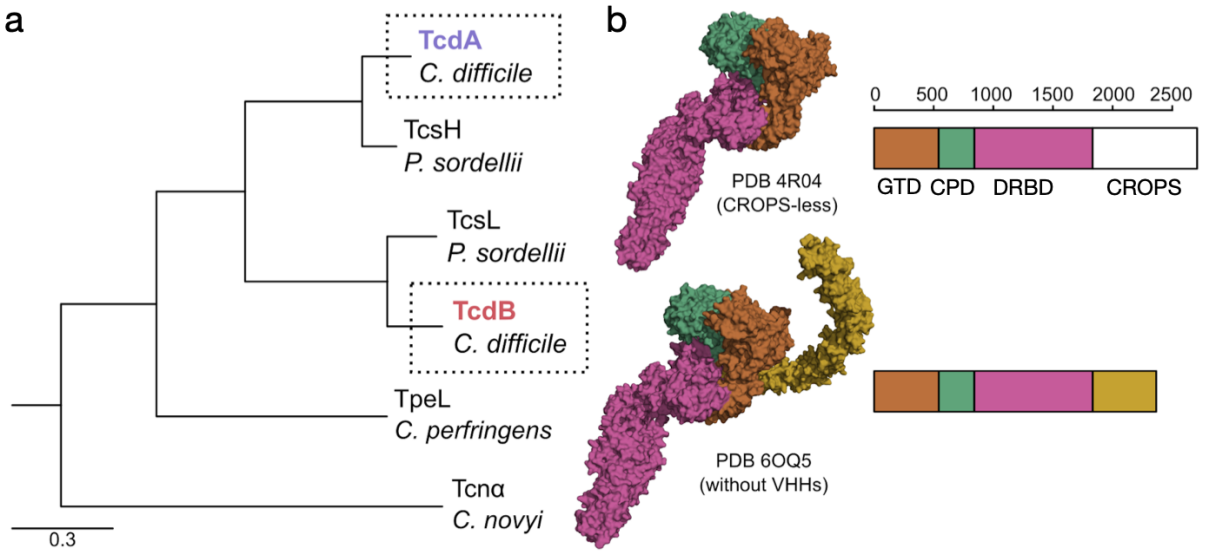

Figure S1. Phylogenetic and structural overview of the TcdA and TcdB protein family. (a) The TcdA family forms a monophyletic clade with TcsH from *Paeniclostridium sordellii* as a sister phylogenetic lineage. Similarly, the the TcdB family forms a monophyletic clade with TcsL from *Paeniclostridium sordellii* as a sister phylogenetic lineage. This implies a scenario whereby TcdA and TcdB evolved by an ancestral gene duplication that predates the speciation event leading to divergence of *C. difficile* and *P. sordellii*. (b) Representative crystal structures and domain architectures are shown for TcdA (above) and TcdB (below). The structure of TcdA lacks the CROPS domain and is derived from PDB ID 4F04. The full-length structure of TcdB is based on PDB ID (6OQ5), and was modified to remove bound antibodies. Domain definitions were derived from Aktories et al.

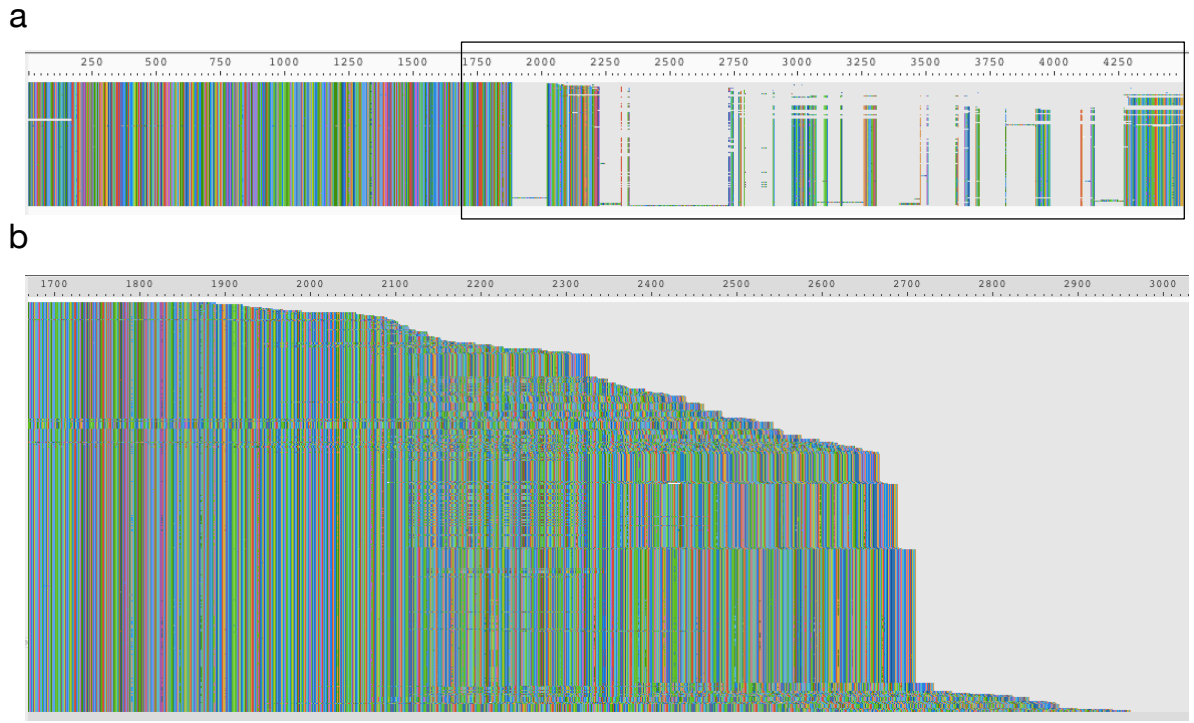

Figure S2. Alignment of TcdA sequences derived from GenBank and the NCBI short read archive, illustrating considerable variation in the length of the C-terminal CROPS region. (a) Complete alignment of 480 unique TcdA sequences. (b) Visualization of unaligned sequences to display C-terminal length variation following residue ~900.

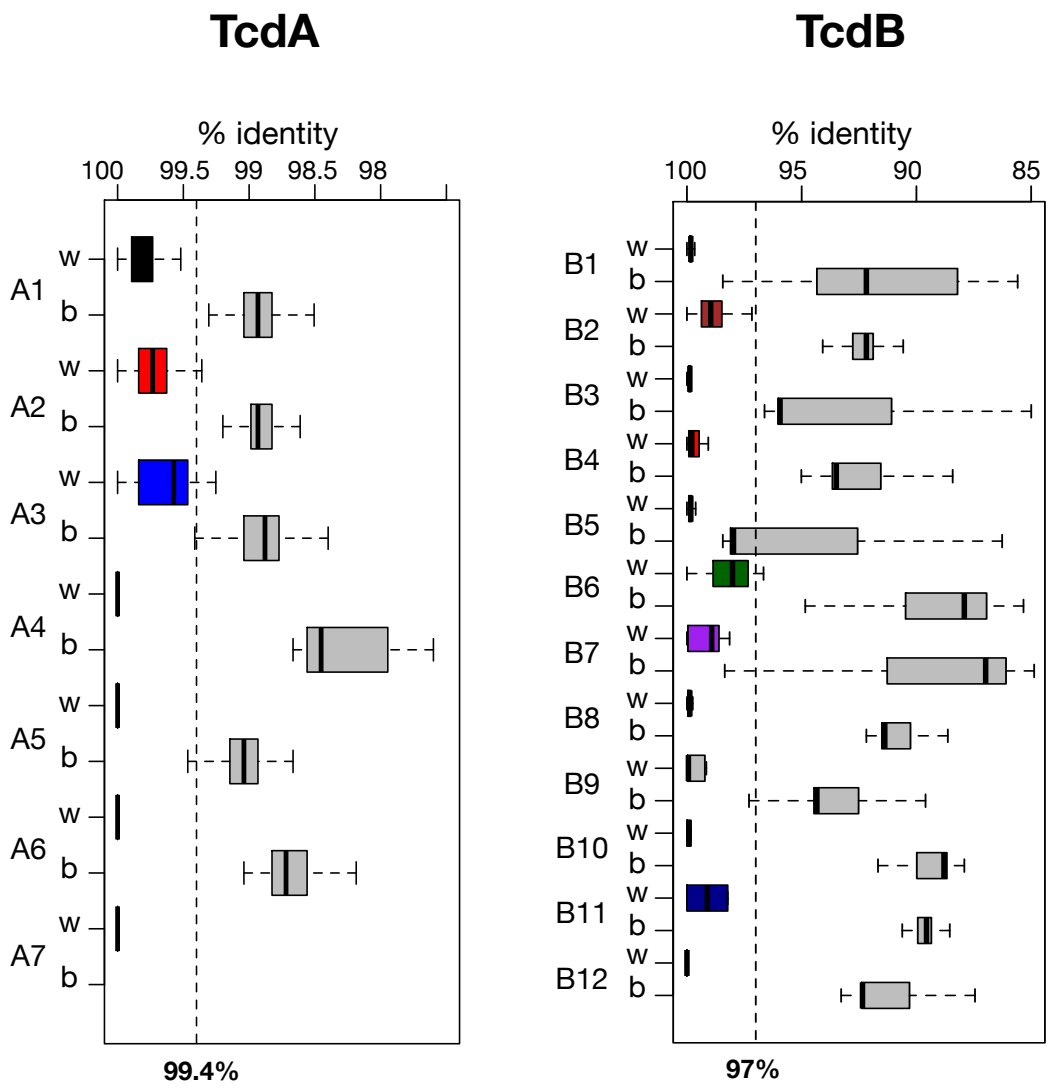

Figure S3. Analysis of sequence similarities within and between subtypes of TcdA and TcdB. Pairwise sequence identities were calculated between all TcdA and TcdB sequences. The % identity distributions are plotted for sequences within ("w") the same subtype versus between ("b") subtypes for TcdA (left) and TcdB (right). As expected, the % identities are much higher within than between subtypes. For TcdA, a % identity threshold of 99.4 effectively distinguishes sequences within the same subtype, whereas for TcdB, a threshold of 97% effectively distinguishes sequences within the same subtype.

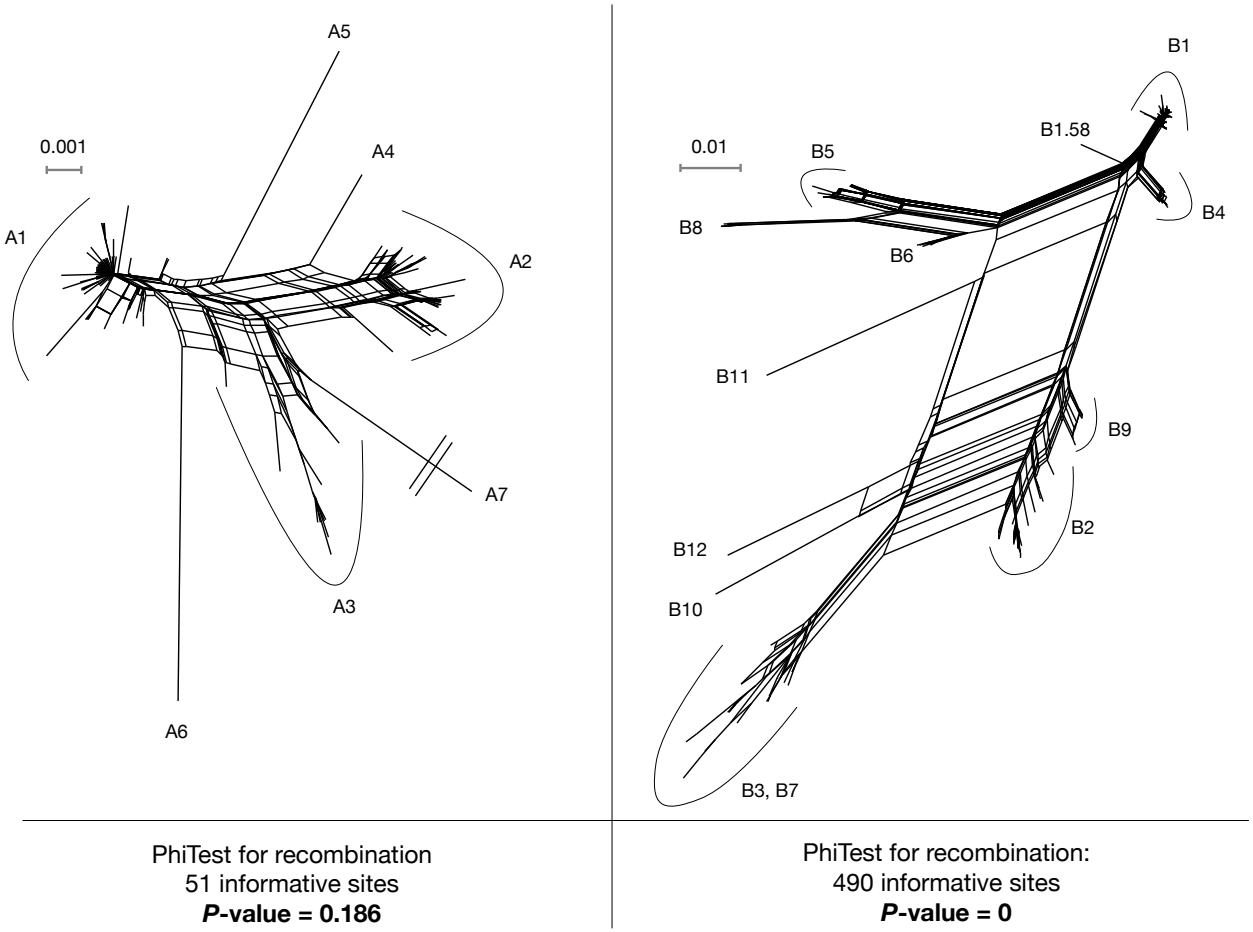

Figure S4. SplitsTree analysis of TcdA and TcdB and statistical detection of recombination. Split networks of TcdA and TcdB were generated using the SplitsTree software. Parallel edges suggest the existence of sites that are not compatible with a perfect monophyletic tree, which can result from recombination. An extremely long branch (A7) has been truncated in order to permit visualization.

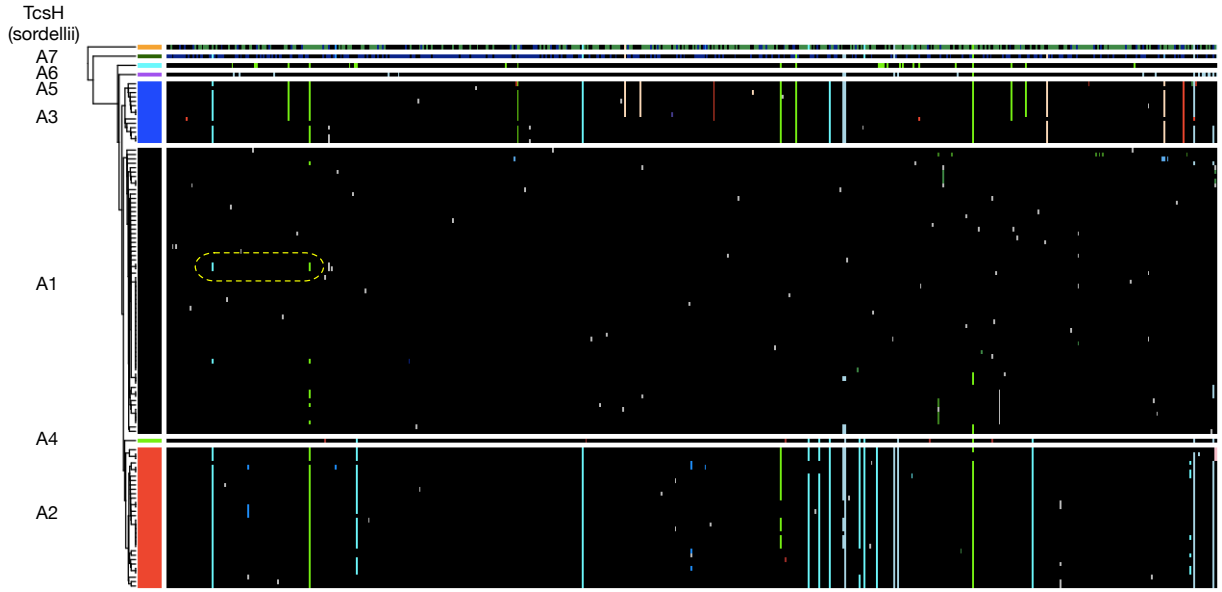

Figure S5. Haplotype analysis of the CROP-less TcdA alignment. Visualization and analysis of amino acid variation patterns was performed using the HaploColor algorithm (https://github.com/doxeylab/haploColor), which was run for 16 iterations. Patterns of amino acid variation within each phylotype are highly homogeneous, and thus a lack of evidence for recombination. One potential exception is highlighted in yellow, involving two amino acid variants that occur within phylotype A1 that are lacking in most other A1 sequences but present in phylotypes A2 and A3. However, this pattern may also be due to ancestral variation rather than recombination. Overall, compared to TcdB, the TcdA displays considerably less sequence variation and lacks the mosaic patterns that would result from recombination.

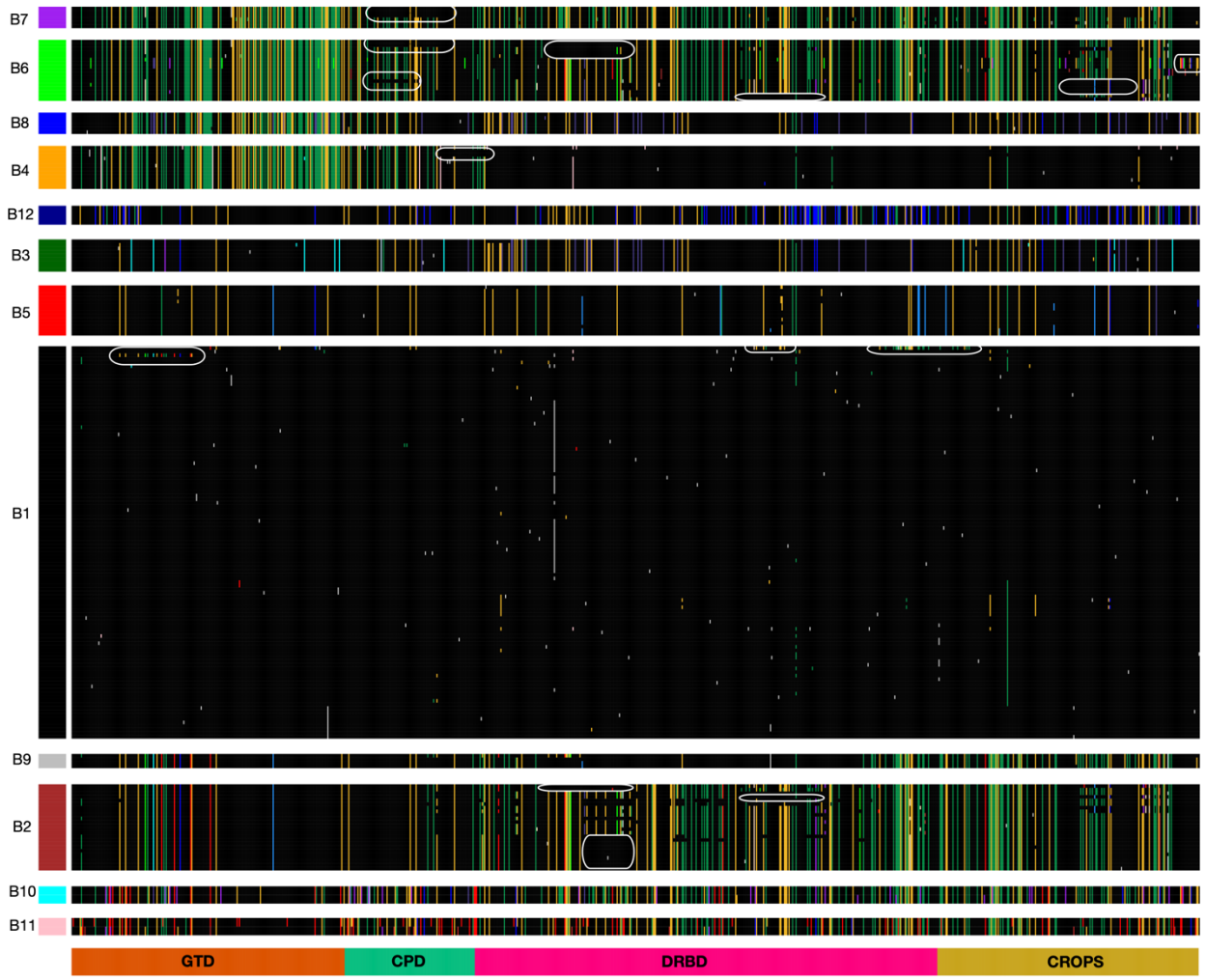

Figure S6. Visualization of amino acid variation patterns in TcdB highlighting putative microrecombination events. The TcdB multiple sequence alignment was colored using the HaploColor algorithm (https://github.com/doxeylab/haploColor), which was run for 16 iterations. Fourteen example segments containing amino acid variants that are unexpected for their subtype are shown by white ovals. These represent putative between-subtype microrecombination events. These fourteen are not a complete list as many more can be seen visually.

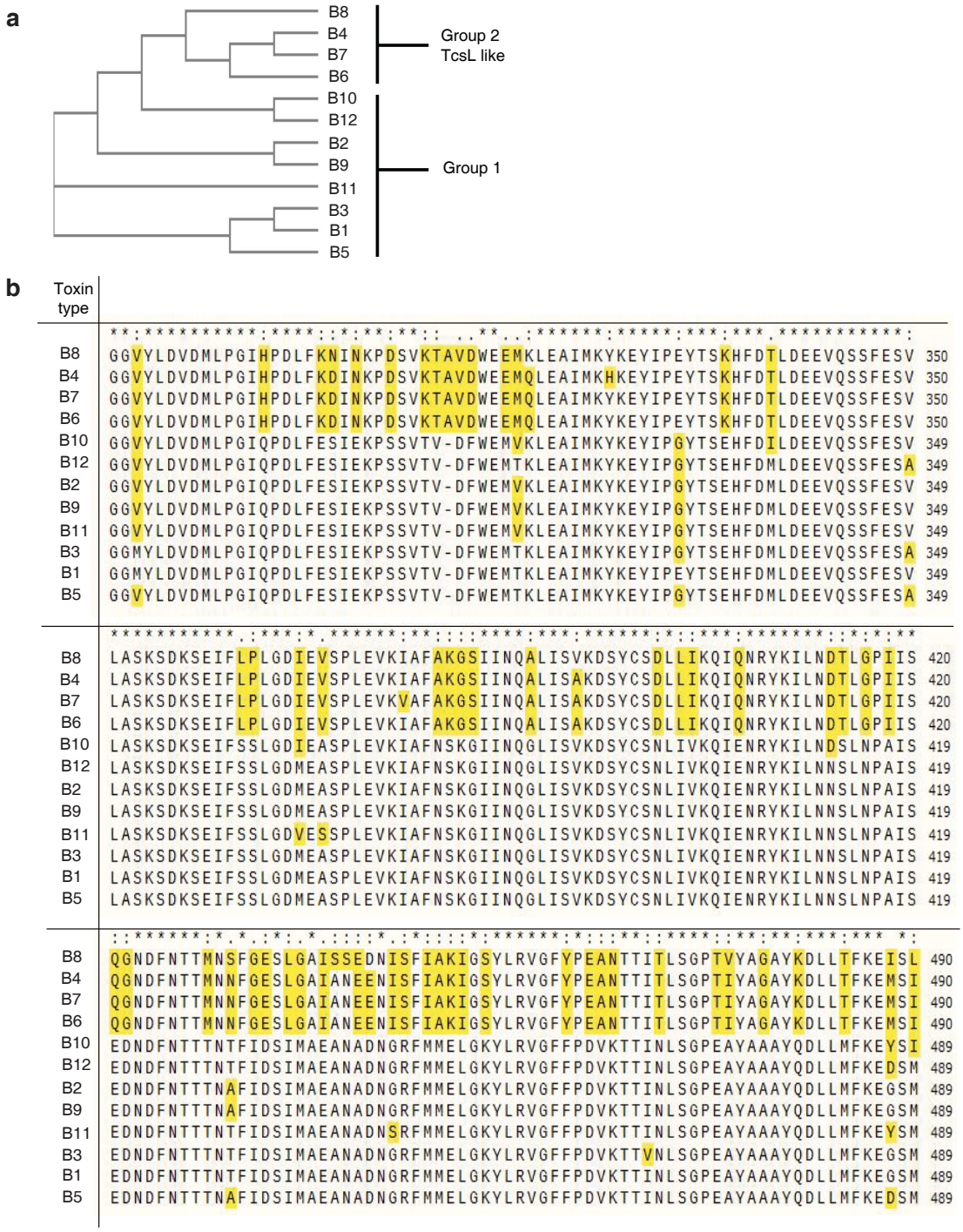

Figure S7. a) Phylogenetic tree of the GTD domains. B) alignment of region 280-490. According to the tree and the alignment, and the functions, GTD domains could be classed into to groups, one group is TcsL-like which gives vero cells rounding and clumping phenotypes (strain 1470 and 8846); the other group is the classical TcdB-like group which only give the rounding phenotype.

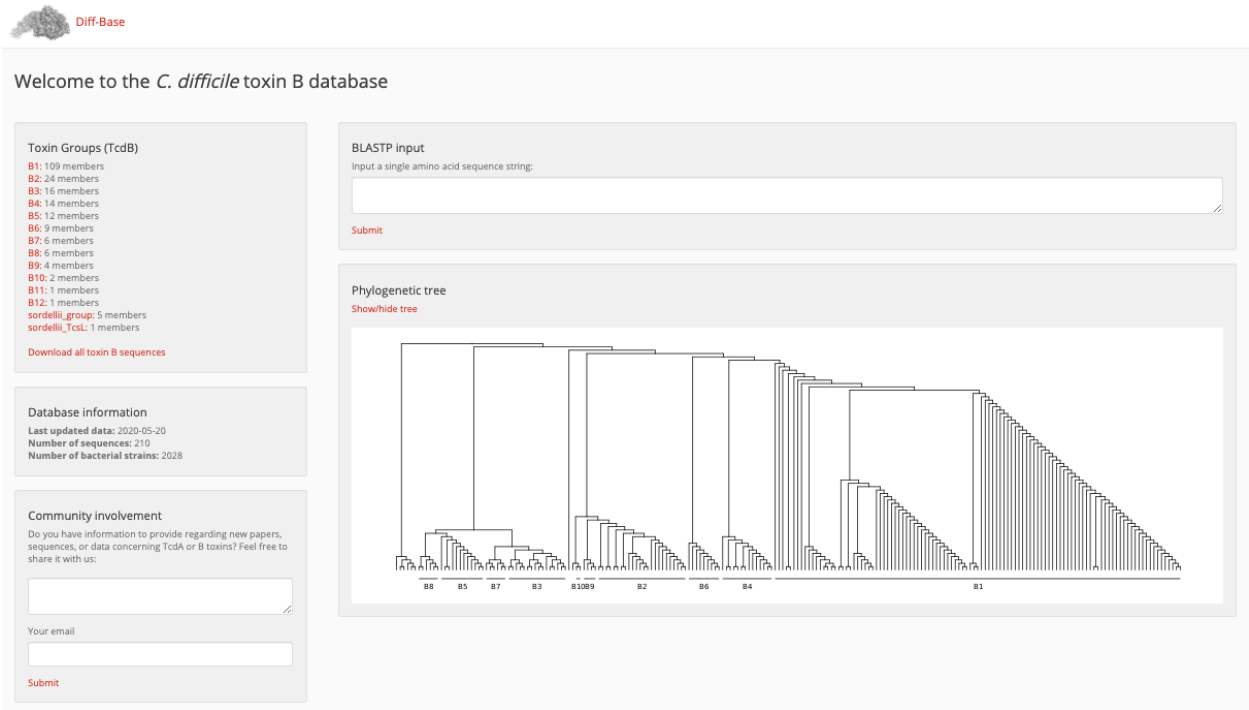

Figure S8. A screenshot of the DiffBase online database.

Table S1. Subtypes of novel TcdA and TcdB sequences identified in the NCBI short read archive. Novel sequences contain at least one substitution not observed in existing sequences derived from NCBI GenBank.

Subtype	**#**
A1	25
A2	10
A3	3
A4	1
A5	1
A6	1
B1	52
B2	12
B3	2
B4	1
B5	2
B6	7
B7	1
B8	4
B9	3

Table S2. List of clinically relevant and previously studied *C. difficile* strains, associated toxin phylotypes, and toxinotypes. Different groups are assigned unique colors. The table is based on information compiled from Rupnik and Janezic (2016), Bletz et al. (2018), and NCBI genome metadata.

Toxinotype	Strain	Ribotype	Clade	TcdA subtype	TcdB subtype	Combined subtype	Toxin Production	Notes
0	VPI 10463	003/087		A1.1	B1.1	A1/B1	A+B+CDT−	TcdB1
0	630	012	1	A1.4	B1.1	A1/B1		TcdB1
0	E28	012		A1.38	B1.1	A1/B1		
0	T3	012		A1.4	B1.1	A1/B1		
0	E14	014/020		A1.1	B1.2	A1/B1		
0	CD166	014/020		A1.1	B1.5	A1/B1		
	CD111	014/020		A1.1	B1.2	A1/B1		
	CD109	014/020		A1.1	B1.2	A1/B1		
	CD90	014/020		A1.1	B1.2	A1/B1		
0	CD43	027			B1.5	-/B1		
0	E12	106		A1.1	B1.4	A1/B1		
0	5555-DH/ST42	002		A1.1	B1.46	A1/B1		
0	CD002	002			B3.1	-/B3		
0/V	597B	131		A1.14	B1.56	A1/B1	A+B+CDT+	
I	EX 623	102	1	A1.1	B1.109	A1/B1	A+B+CDT+	
II	AC 008	103	1	A1.1	B1.3	A1/B1	A+B+CDT+	
III	R20291	027	2	A2.1	B2.1	A2/B2		TcdB2
IIIb	R 12087 (=CD196)	027	2	A2.1	B2.1	A2/B2	A+B+CDT+	
IIIa	SE 844	080	2	A2.5	B9.1	A2/B9	A+B+CDT+	
IIIc	CH6230	251	2	A2.7	B2.3	A2/B2	A+B+CDT+	
IIIe	AI 541	251	2	A2	B2.7	A2/B2	A-B+CDT+	
IIId	3073	SLO 042	2	A2.11	B2.24	A2/B2	A+B+CDT+	
IV	55767	023	3	A3.2	B5.1	A3/B5	A+B+CDT+	
V	SE 881	045	5	A3.4	B3	A3/B3	A+B+CDT+	
V	M120	078	5	A3.1	B3.1	A3/B3		
	NAP07	078		A3.1	B3.1	A3/B3		
VI	51377	127	5	A3.1	B3.1	A3/B3	A+B+CDT+	
VII	57267	063	5	A3.1	B3.7	A3/B3	A+B+CDT+	
VIII	1470	017	4		B4.1	-/B4	A−B+CDT−	
VIII	M68	017			B4.1	-/B4		
VIII	E13	017			B4.1	-/B4		
IXa	51680	019	2	A2.2	B6.1	A2/B6	A+B+CDT+	
Ixb	TFA/V20-1	244	2	A2.6	B6.2	A2/B6		
IXc	8785	109	5	A2	B6.5	A2/B6	A+B+CDT+	

IXd	1732874	SLO 228	2	A2.8	B6.13	A2/B6	A+B+CDT+
Xa	8864	036 / 591(CE)	2		B7.1	-/B7	A−B+CDT+
Xb	J9965	SLO 032	2		B7.4	-/B7	A−B+CDT+
XIa	IS 58	033	5			-/-	A−B−CDT+
XId	OCD 5/2	033	5			-/-	A−B−CDT+
XIb	R 11402	288 (CE)	5			-/-	A−B−CDT+
XII	TFA/V14-10	153(CE)	2			-/-	A−B−CDT+
XII	IS 25	258	1	A1.1	B1.10	A1/B1	A+B+CDT-
XIII	R 9367	070	1		B1.2	-/B1	
XIVa	R 10870	111	2	A2	B6.3	A2/B6	A+B+CDT+
XIVb	R 9385	122	2	A2.12	B6.6	A2/B6	A+B+CDT+
XVI	SUC36	078	5	A3.8	B3.6	A3/B3	A+B+CDT+
XVIII	K095	014	1	A1.1	B1.105	A1/B1	A+B+CDT−
XIX	TR13	018	1	A1.2	B1.2	A1/B1	A+B+CDT−
XX	TR14	SLO 005	1	A1.1	B1.16	A1/B1	A+B+CDT−
XXI	CH6223	SLO 035	4	A1.35	B4.11	A1/B4	A+B+CDT−
XXII	CD07-468	027	2	A1.36	B2.1	A1/B2	A+B+CDT+
XXV	7325	027	2	A2.1	B2.1	A2/B2	A+B+CDT+
XXVI	7459	050 (CE)	1		B1.6	-/B1	A-B+CDT−
XXVII	KK2443/2006	SLO 037	1			-/-	A-B-CDT−
XXVIII	CD08-070	126	5	A3.1	B3.1	A3/B3	A+B+CDT+
XXIX	CD07-140	001	1	A1.1	B1.2	A1/B1	A+B+CDT−
	CD92	001		A1.1	B1.2	A1/B1	
XXX	ES 130	SLO 101	5		B8.1	-/B8	A-B+CDT+
XXXI	WA 151	SLO 098			B8.2	-/B8	A-B+CDT+
XXXII	173070	151(CE)	C-II		B12.1	-/B12	A-B+CDT-
XXXIII	2402	SLO 086	1	A1.37	B4.10	A1/B4	A+B+CDT-
XXXIV	CD10-055	SLO 201			B2.7	-/B2	A-B+CDT-
XXXIII	2402	SLO 086		A1.37	B4.10	A1/B4	A+B+CDT-
	RA09-70			A7.1	N	A7/-	A+B-CDT-
	CD160				B11.1		
	HMX-149			N	B11.2	-/B11	A-B+CDT-
	CD10-165		C-I	N	B10.1	-/B10	A-B+CDT-
	SA10-050		C-I	N	B10.2	-/B11	A-B+CDT-
	HSJD-312			N	B6.9	-/B6	A-B+CDT+
	HMX152			N	B6.9	-/B6	A-B+CDT+